Geochemistry 86 (2026) 126364

Contents lists available at ScienceDirect

Geochemistry

journal homepage: www.elsevier.com/locate/chemer

Mineralogy, geochemistry and genesis of newly discovered Sinandede kaolin deposit (Balıkesir, NW Türkiye): Potential applications

Fazlı Çoban [a], Şenel Özdamar [b,*], Oral Sarıkaya [b], Gökhan Büyükkahraman [a], Zeynep Döner [b], Naşide Merve Sütçü [b]

[a] Balıkesir University, Department of Geological Engineering, Balıkesir, 10145, Türkiye
[b] Istanbul Technical University, Department of Geological Engineering, İstanbul, 34469, Türkiye

ARTICLE INFO

Handling Editor: Xiaochun Li

Keywords:
Hydrothermal alteration
Isotope
Kaolin
Mineralogy
NW Türkiye
Sinandede

ABSTRACT

This paper presents first X-ray diffraction (XRD), scanning electron microscopy (SEM), bulk-rock geochemical analyses, isotopic (O-H-C) and differential thermal analysis-thermogravimetric (DTA-TG), physical and thermal tests of Sinandede kaolin deposit (SKD) formed by hydrothermal alteration of Lower Miocene dacitic-rhyodacitic tuffs. The mineralogical analyses revealed that the SKD comprises mainly kaolinite with dickite, illite, smectite-chlorite, Ca-montmorillonite, alunite, halloysite, feldspar, quartz, opal CT, hematite and anhydrite. Geochemically, Al_2O_3, H_2O, Sr, S and Zr contents were markedly enriched, while Rb, Cs, U, Y and Ba were depleted compared with the parent rocks. The chondrite-normalized rare earth element (REE) patterns show identical trends characterized by light rare earth element (LREE) enrichment $(La/Sm)_{CN} = 1.96–10.96$ and $(La/Yb)_{CN} = 20.51–37.08$), heavy rare earth element (HREE) depletion $(Gd/Yb)_{CN} = 1.37–5.62$), slightly Eu anomaly ($Eu/Eu^* <1$), and positive Gd anomaly ($Gd/Gd^* =$ av.1.06). The $\delta^{18}O$ values of the samples vary between +0.48 ‰ and, −4.96 ‰; δD values vary between −81.05 ‰ and − 89.97 ‰. On the other hand; $\delta^{13}C$ (VPDB) values ranging between −25.70 ‰ and − 28.83 ‰ (VPDB) in kaolin samples are compatible with the $\delta^{13}C$ (VPDB) values of hydrothermal waters mixed with meteoric water fed by C3 plants, indicating the contribution of meteoric water in SDK. Small positive Ce and Gd anomalies, which indicates the presence of a hypogene-supergene mix, further support the contribution of meteoric water. The SDK was formed as a result of post-magmatic hydrothermal activities at temperatures above 100 °C and influenced by both hypojene and supergene conditions. Technological tests suggest that the SDK can be used for wall and floor tiles in ceramic industry.

1. Introduction

Kaolinite clays are important raw materials that are the main component of glazed or unglazed porcelain tile products (Çoban et al., 2002; Das et al., 2005; Yanık et al., 2010 references therein; Dill, 2016). Kaolinite, higher than 50 %, is the main mineral in kaolin, recognized for its unique properties, especially used in industries such as ceramics, paper and paint. Kaolinization is of two types as primary and secondary (Dill, 2016). Kaolin is the type-lithology of the near-surface continental environments (Dill, 2016; Ekinci Şans et al., 2025). However, some authors suggest that kaolin deposits were formed in swampy environments rich in organic matter (Spears and Kanaris-Sotiriou, 1979; Çoban et al., 2012).

Several researchers have reported hydrothermal and weathering type kaolin deposits that can be economically exploited in Türkiye (Yanık et al., 2018; Laçin et al., 2021; Çelik Karakaya et al., 2021; Ünal Ercan et al., 2022; Kadir et al., 2022). Western Anatolia hosts Cenozoic aged volcanic products with calc-alkaline character showing compositional variations between basalt and rhyolite. Economic kaolin deposits have developed throughout the region because of hydrothermal alteration of these volcanic products (Sayın, 2007; Ece et al., 2013; Çoban, 2015).

The above-mentioned researchers have made significant contributions to our understanding of kaolin deposits formed by hydrothermal alteration in the Western Anatolia. Sinandede kaolin deposit formed because of hydrothermal alteration of Lower Miocene rhyodacite-dacite (occasionally trachyandesite) composite tuffs is located southwest of Sinandede village (Sındırgı-Balıkesir) on the 1:25,000 scale Balıkesir J20-d1 topographic map. Sinandede kaolin deposite was neither tested for ceramic application nor academic viewpoint. This study investigated

* Corresponding author.
E-mail address: ozdamarse@itu.edu.tr (Ş. Özdamar).

https://doi.org/10.1016/j.chemer.2025.126364
Received 3 July 2025; Received in revised form 27 November 2025; Accepted 28 November 2025
Available online 30 November 2025

the mineralogical, geochemical characteristics and technological properties of this clay deposit for the first time to reveal its genesis and possible ceramic applications.

2. Materials and methods

X-Ray diffraction (XRD) for mineralogical composition, optical microscope, scanning electron microscope (SEM) for petrographical properties, whole rock major, trace and rare earth elements analyses for clay and bedrock geochemistry and stable isotope (δD, $\delta^{18}O$ and $\delta^{13}C$) for genesis of samples, thermogravimetry-differential thermal analysis (DTA-TG) for thermal features and technological tests were carried out on samples taken systematically from volcanic rocks associated with kaolin formation and kaolin deposits. To elucidate the spatial variability within the Sinandede kaolin deposit, a schematic diagram (Fig. 1c) was developed. This figure delineates the relative positions of the upper, middle, and lower sections of the deposit, as well as the north-northeast and south-southwest extensions of the deposit. In addition, sampling points (SDK numbers) were plotted to clarify their spatial distribution in relation to the principal geological units. A total of 29 samples were systematically collected from the Sinandede kaolin deposit and adjacent volcanic rocks. This collection includes 6 kaolin samples for physical testing, 8 samples (comprising 7 kaolin and 1 parent rock) for comprehensive chemical analysis, 5 kaolin samples for stable isotope analysis, 2 representative kaolin samples for XRD analysis, 3 kaolin samples for DTA-TG analysis, and 5 kaolin samples for SEM-EDX examination. The sample codes (SDK) referenced throughout the manuscript correspond to those presented in the analytical data tables and figures. Table 1 provides detailed information on each sample, including lithology, location, depth (for drill cores), and analytical method employed. Petrographic investigations were performed with Olympus CX31-P polarizing microscope in the optical mineralogy laboratory of the Department of Geological Engineering, Faculty of Engineering, Balıkesir University. XRD analyses were carried out at Afyon Kocatepe University, Technology Research Center with Shimadzu XRD-6000 model x-ray diffractometer (Ni-filtered, Cu-Kα radiation); normal, ethylene glycol and 400 °C baked XRD shots were obtained on clay size samples. 2 kaolin samples with different mineralogical compositions were coated with thin carbon film at 250–300 Å and examined with LEOVP-1431 model SEM analysis at Afyon Kocatepe University Application and Research Center (AKU-TUAM). Chemical analyses for major, trace and rare earth elements were performed at Acme Analytical Laboratories

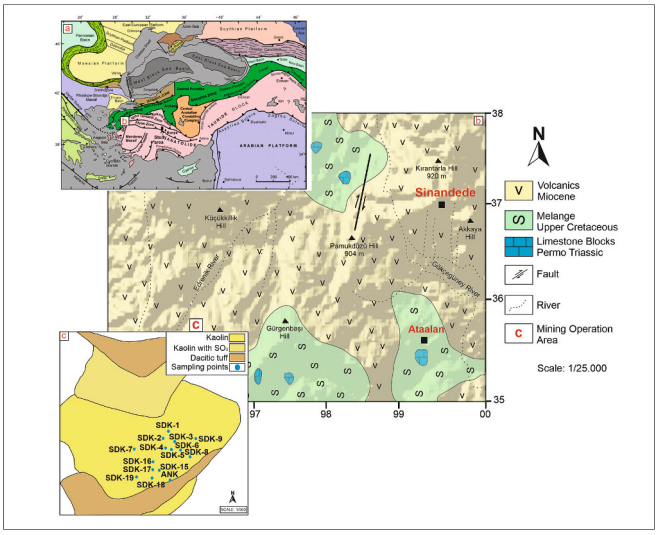

Fig. 1. a) Neo-tectonic map of Türkiye (from Okay and Tüysüz, 1999), b) Geological map of the study area (modified from Çoban et al. (2011)), c) Geological map of the mining operation area.

Table 1
Sample list and analytical methods applied to the Sinandede kaolin deposit.

Sample No	Lithology	Analysis Type(s)
SDK-1	Kaolin	Physical test, Chemical analysis, DTA-TG
SDK-2	Kaolin	Physical test, Chemical analysis
SDK-3	Kaolin	Physical test, Chemical analysis, DTA-TG
SDK-4	Kaolin	Physical test
SDK-5	Kaolin	Physical test, DTA-TG
SDK-6	Kaolin	Physical test, XRD
SDK-7	Kaolin	SEM
SDK-8	Kaolin	XRD
SDK-9	Kaolin	SEM
SDK-14 (ANK)	Parent rock	Chemical analysis
SDK-15	Kaolin	Stable isotope analysis, Chemical analysis, SEM-EDX
SDK-16	Kaolin	Stable isotope analysis, Chemical analysis, SEM-EDX
SDK-17	Kaolin	Stable isotope analysis, Chemical analysis, SEM-EDX
SDK-18	Kaolin	Stable isotope analysis, Chemical analysis
SDK-19	Kaolin	Stable isotope analysis

(ACME-Canada). ICP-ES (Inductively Coupled Plasma-Emission Spectrometry) method was applied for main oxide analysis and ICP-MS (Inductively Coupled Plasma-Mass Spectrometry) method was applied for trace element (TE) and rare earth element (REE) analysis. For ICP-MS analyses, approximately 200 mg of powdered sample was digested using 10 mL of concentrated HNO_3 in closed Teflon beakers on a hot plate at 150 °C for 48 h. After complete dissolution, the solutions were evaporated to dryness and then redissolved in 2 % HNO_3 prior to measurement. Procedural blanks and international rock standards (BHVO-2, AGV-2) were processed simultaneously to monitor data quality. S0–15 standard was used in the determinations of some of the trace elements and rare earth elements (Pickering et al., 1993). For the purpose of conducting stable isotope analyses, 5 representative kaolin samples were initially purified to isolate kaolin-rich components. The bulk clay fractions underwent a series of treatments, including the removal of organic matter using 10 % H_2O_2, dissolution of carbonates with 0.1 N HCl, and dispersion achieved through repeated washing and centrifugation. The fraction smaller than 2 μm was separated using sedimentation. Dickite, illite, and smectite-chlorite mixtures were minimized by carefully selecting samples that exhibited dominant kaolin peaks in the XRD patterns and by repeated sedimentation until the XRD reflections confirmed kaolin-dominant compositions. These purified components were then used for $\delta^{18}O$ and δD measurements. Samples were analysed by Delta V Advantage model Thermo Fisher Isotope Mass Spectrometer at Cornell University (USA) stable isotope laboratory. DTA-TG analyses of 3 kaolin samples were carried out with Netzsch STA 409 PC/PG Thermogravimetric Analyzer at Eskisehir Anadolu University Ceramic Research Center under the conditions of heating rate 10 °C/min, paper speed: 10 mm/min were performed with Netzsch STA 409 PC/PG brand Thermogravimetric Analyzer at Eskişehir Anadolu University, Ceramic Research Center. Firing shrinkage and firing strength parameters were examined in Uşak Ceramic factories and moisture, viscosity, sieve balance, shrinkage, water absorption, glow loss and color parameters were examined in Thermal Ceramic laboratories. For firing shrinkage and firing strength parameters, 1188 °C temperature was applied for 33 min and 1203 °C temperature was applied for 35 min for other parameters.

3. Geology and petrography

Türkiye is located in the Alpine-Himalayan orogenic belt, between the Anatolian block and the Eurasian and Arabian plates. The neotectonic process in Türkiye is characterized by continental collision between the Eurasian and Arabian plates, which caused crustal thickening and contraction in western Anatolia (Dewey, 1988). Therefore, the Anatolian block began to escape westward along the North

Anatolian fault (right-lateral fault) and the East Anatolian fault (left-lateral fault) (McKenzie, 1972; Fig. 1a). The escape of the Anatolian block was terminated by the Helen shear zone in the Aegean region and N-S extension caused by east-west compression (Şengör and Yilmaz, 1981).

The Sinandede kaolin deposit is located within the Lower Miocene dacitic–rhyodacitic pyroclastic unit, occasionally interspersed with trachyandesitic tuffs. An analysis of 13 boreholes drilled in the region revealed that the thickness of kaolin ranges from 6.25 to 40 m, with the altered zones frequently exhibiting silicification and occasional enrichment with Fe—Mn oxides. The integration of field mapping and drill core logging elucidated the vertical and lateral variations in kaolinization processes.

According to the studies conducted in different parts of Western Anatolia, the volcanic rocks are divided into two groups as dominant andesite and basic rocks (Ünal, 1972). The group including calc-alkaline, highly calc-alkaline and shoshonitic rocks developed due to the compressional regime. Basaltic volcanism, on the other hand, is alkaline and developed toward the end of the Late Miocene when N-S compression was replaced by N-S extension (Garbarino et al., 1994). In addition, there are also opinions that N-S tensional tectonics started in the Late Oligocene-Early Miocene and that the Oligocene-Pliocene volcanic activity in the Aegean Sea developed entirely under the tensional regime (Seyitoglu et al., 1992).

The study area is located within Balıkesir J20-d1-d2 topographical sheets and cover an area of approximately 15 km^2 southwest of Sinandede village (Fig. 1b). Rocks belonging to the Upper Cretaceous Bornova Flysch Zone (Complex Series-Melange (Okut et al., 1978) consisting of a complex of serpentinite, harzburgite, dunite and diabase dykes containing Permo-Triassic aged crystallized limestone blocks form the basement of the study area (Akdeniz and Konak, 1979). The underlying rocks are brown and abundantly fractured serpentinized harzburgite, showing typical alteration. Serpentinites are light-dark greenish-brown colored, abundantly fractured. Diabase dykes outside the study area (Çoban et al., 2011) cut the unit, which is filled with calcite and sometimes magnesite in its fractures.

It was determined that the Miocene aged (Ercan et al., 1984) volcanic rocks unconformably overlying the basement have a volcanic arc type formation concurrent with the collision and the high potassium calc-alkaline rocks are mainly composed of rhyolite, dacite and andesitic-trachyandesitic lavas and their pyroclastics (Çoban et al., 2011; Çoban et al., 2012). Geochemical studies show that the volcanics that formed the kaolin formations were formed from a subalkaline magma of trachyte-trachyandesite composition; while the negative Nb anomaly indicates subduction and/or crustal influence during the development of the magma. High Rb, Ba, and Zr contents indicate that magma contamination occurred during differentiation (Çoban et al., 2012). The volcanic rock assemblage is similar to the Early Miocene aged "Sındırgı volcanic unit" (dacitic and rhyolitic intrusions, lavas and pyroclastic rocks) described by Erkül et al. (2005) in the Bigadiç-Sındırgı region.

The dacite and rhyodacite lavas whose typical outcrops are observed in Kocakillik and Killik hill region (Fig. 1b) in the study area are fractured and fragmented. The lavas, whose coarse feldspars are visible, are reddish-burgundy-purple colored in places. The dacite lavas in the south-southwest parts of the kaolin quarry generally contain roundish-ellipsoidal, 3–5 cm. wide and 8–10 cm. long dark colored enclaves reflecting the basic composition. It was determined that the dacite and rhyodacite lavas are semi-crystalline-semi-glassy, microlitic porphyritic, hyaloplitic, fluidal in texture and contain 20–30 % quartz, 10–20 % plagioclase (oligoclase-andesine), 0–10 % alkali feldspar (sanidine), 5–8 % biotite, 3–9 % amphibole (hornblende), maximum 3 % opaque minerals (hematite, pyrite), and 0–2 % augite. In the dacitic samples, quartz, large sanidine, and plagioclase phenocrysts are irregularly distributed in different sizes in a glass-rich matrix. In the western parts of the region, glassy paste is dominant in the hard and silicified trachyandesites covering N75W/5O^{o}W directional fractures.

Sinandede kaolin deposit located at coordinates 96,319/35754 southwest of Küçükkillik hill in the study area was formed as a result of hydrothermal alteration of Lower Miocene aged dacite-rhyodacite and sometimes trachyandesitic composite tuffs. The green-brown, sandy tuffs are heavily altered, silicified and kaolinized in the upper parts. Plagioclase (albite-oligoclase), quartz, alkali feldspar (orthoclase, sanidine), and a small amount of biotite are the primary minerals in the tuffs consisting mainly of glassy matrix and crystal fragments. Generally fractured feldspars are chloritized, carbonatized, kaolinized, biotite, and hornblende, which are rarely included in the composition, are chloritized. In addition to these, small pumice fragments are occasionally included in the composition. Kaolin formation is occasionally found in dacitic-rhyodacitic tuffs with pumice characteristics. Kaolinization is in the form of veins, irregular pockets, complete kaolinization of feldspar and glassy material or kaolinization in voids in pumice-characterized sections.

Field observations show that the white, grayish beige colored kaolins containing dacitic tuff levels can be classified as soft and the light brownish kaolins as hard and sandy in places. In the upper sections, iron-manganese yield is observed along the fracture lines-oriented D—B to the west and N30^{o}E/85^{o}NW to the east of the kaolin deposit, which is 3–6 m thick and very hard, intensely fractured, light brownish-yellow colored, containing silicified zone containing dense iron-manganese oxide on the fracture surfaces (Fig. 2).

According to 13 drillings, the thickness of kaolin varies between 6.25 and 40 m in an area of approximately 13,000 square meters and the thickness increases from north to south. The kaolin, which is ferrous in the upper parts and sulfurous (SO_3) in the middle parts, is silicified between 2 and 10 m. Kaolin contains silicified zones with an average thickness of 4.5 m at different depths (between 5th and 35th meters) and contains volcanic rock fragments with a thickness ranging between 0.5 and 1 m (Çoban et al., 2011).

4. Results

4.1. XRD analysis

The whole rock-clay size mineralogical compositions of the samples collected from the Sinandede kaolin deposit were determined by XRD investigations. The main clay minerals identified are kaolinite, alunite, halloysite, dickite, illite, smectite-chlorite, and Ca-montmorillonite. Non-clay minerals are feldspar, quartz, opal-CT, hematite, and anhydrite. Although kaolin, dickite, and halloysite generally exhibit similar X-ray diffraction (XRD) patterns, they can be distinguished by their specific diagnostic reflections. Kaolin is characterized by its distinct sharp basal reflections at 7.15 Å (001) and 3.58 Å (002). In contrast, dickite is identified by additional unique peaks at 2.29 Å and 1.54 Å, which are absent in kaolin. Halloysite is distinguished by a broad and less intense reflection at approximately 10 Å, which is indicative of its tubular structure and partial hydration. In the Sinandede samples, the presence of dickite was confirmed by the 2.29 Å reflection, whereas halloysite was detected only in samples near the surface, as indicated by a broad 10 Å peak. These distinctions, as illustrated in Fig. 3, are consistent with the scanning electron microscopy (SEM) observations and differential thermal analysis-thermogravimetric (DTA-TG) data, further corroborating the identification of the clay mineral phases (Fig. 3). According to the degree of kaolinite crystallization proposed by Wilson (1987), kaolinites in the samples examined mostly show good-medium crystalline properties.

Quartz, one of the silica minerals, is present in the composition of most samples in clay size and has the characteristics of low quartz (alpha quartz) (Brown and Brindley, 1980). Opal-CT; commonly associated with medium-poor crystalline kaolinites; was identified by (101) surface reflections ranging from 4.03 to 4.04 Å (Williams et al., 1985); and alunite; commonly associated with kaolinite + quartz paragenesis; was identified by peaks at 5.70–5.72, 4.96, 2.96, and 2.29 Å in XRD analyses

Fig. 2. a) Kaolin quarry (gray cut altered tuffs on top, kaolin on the bottom), b) Iron-manganese oxide in kaolinization and cracks, c) Iron oxide in cracks, d) Silicified cut on kaolin bed.

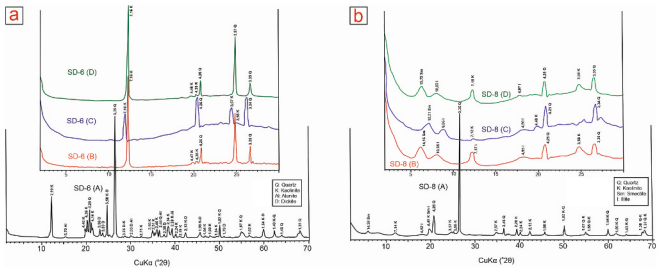

Fig. 3. Representative XRD patterns of kaolin samples from the Sinandede deposit. a) X-ray diffractograms of kaolin sample SD-6, b) X-ray diffractograms of kaolin sample SD-8 (A: whole rock, B: clay size, C: 400 °C heated, D: ethylene glycol saturated). Diagnostic peaks are labeled with the corresponding mineral phases: quartz (Q), kaolin (K), dickite (D), halloysite (H), illite (I), and smectite–chlorite (Sm). The identification of these phases is based on their characteristic basal reflections (e.g., kaolin at 7.15 and 3.58 Å, dickite at 2.29 and 1.54 Å, halloysite at ~10 Å) and is consistent with SEM and DTA-TG data.

(Fig. 3). Dicite-quartz paragenesis is typical in areas of high kaolinization (Grecco et al., 2012). Alunite [$KAl_3(SO_4)_2(OH)_6$] is identified by its typical reflections at 5.77, 5.72, 4.96, 3.49, 2.99, 2.89, 2.29, 1.92 Å in XRD studies (Williams et al., 1985). In the XRD diagrams obtained from the samples studied, alunite was identified with peaks at 5.70–5.72, 4.96, 2.96 and 2.29 Å. Alunite is usually associated with kaolinite + quartz paragenesis.

4.2. SEM analysis

Typical pseudo-hexagonal shapes of kaolinite crystals are variable in size, irregularly distributed, and book-shaped aggregates (Figs. 4a, b). The size of the kaolinite crystals is related to the pore size, and the packets formed by the plates are loosely textured. The average size of the kaolinite crystals is 3–8 μm and the thickness of the aggregates is 30–40 μm. It has been determined that the matrix material in which kaolinite is found has two distinct properties: fine-grained (Fig. 4c) and gel-like. Accordingly, the matrix material in which both the book-shaped and irregularly distributed kaolinites developed is fine-grained and contains iron and titanium (Fig. 4d). In the alunite samples, kaolinite crystals developed as flakes with less thickness, and the intermediate material in which kaolinite crystals are found is gel-like and rich in SO_3 (40.40 %) (Figs. 4e, f). Alunite developed from this gelatinous material (Fig. 4g). The high content of SO_3 in the gel-like material is remarkable (Fig. 4h).

4.3. Thermal analysis

DTA-TG curves of the kaolin samples examined are given in Fig. 5.

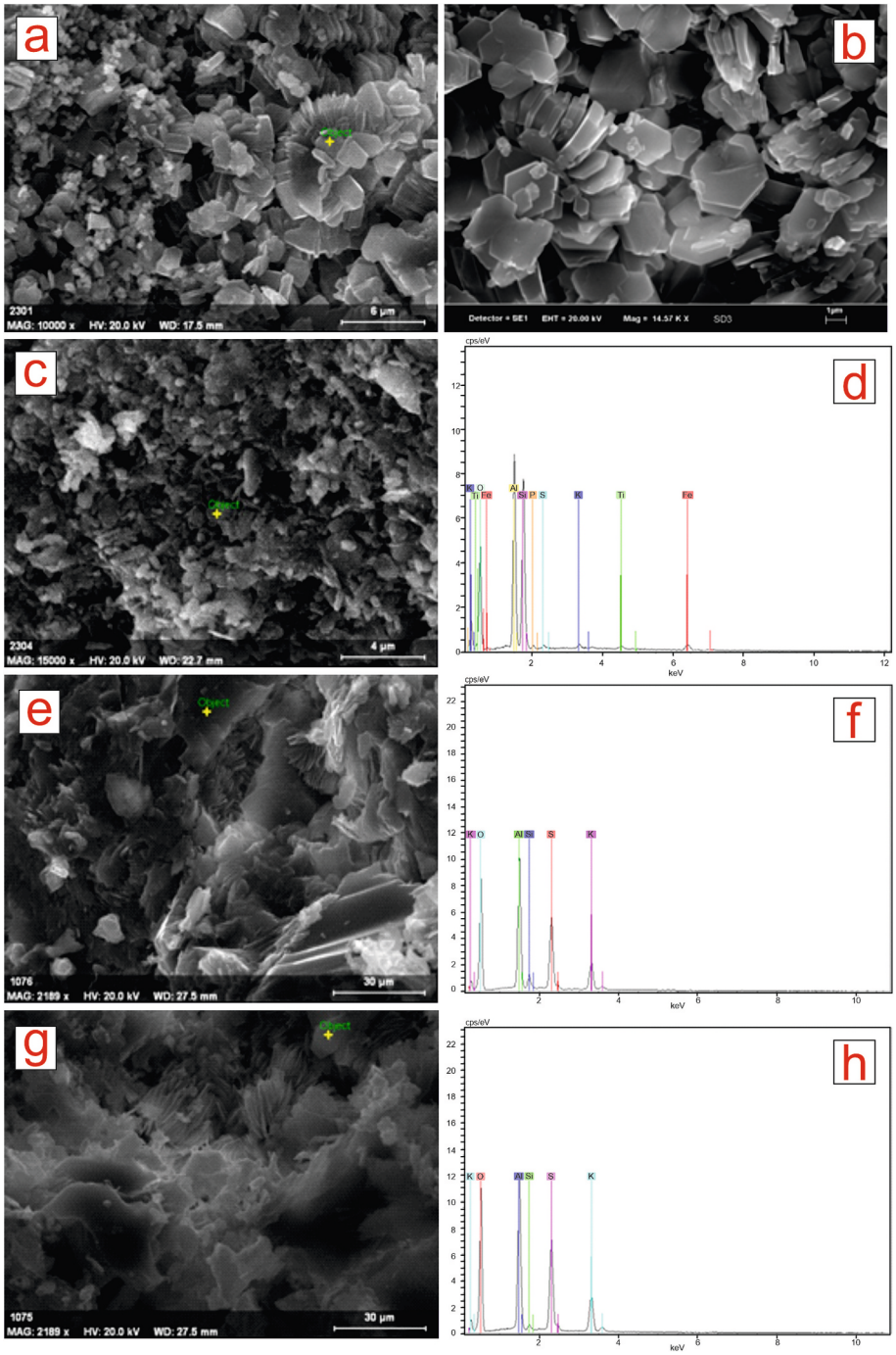

Fig. 4. SEM images of Sinandede kaolinite samples a) book-shaped kaolinite agglomerates, b) irregularly distributed pseudo-hexagonal kaolinites, c) fine-grained matrix containing kaolinites, d) Energy distribution (ED) spectrum of the matrix and analysis result (% SiO_2: 50.70, Al_2O_3: 42.41, Fe_2O_3: 3.66, TiO_2: 1.21, K_2O: 1.08, SO_3: 0.48, P_2O_5: 0.46). e-h) SEM images and energy dispersive (ED) spectra of alunite kaolinite samples (e: fine-grained kaolinite crystals in the form of flakes and alunitization developed along the pores in the gelatinous matrix, f: energy dispersive spectrum and analysis result of the gelatinous material (SiO_2: 5. 80 %, Al_2O_3: 41.06 %, SO_3: 40.40 %, K_2O: 12.74 %), g: fine kaolinite crystals, gelatinous matrix and alunitization through the gelatinous matrix, h) ED spectrum result of the analysis of the (+) marked section (SiO_2: 1.24 %, Al_2O_3: 38.36 %, SO_3: 44.67 %, K_2O: 15.73 %).

Accordingly, adsorbed water (H_2O) losses in kaolin samples occur at around 100 °C and considering the peak at 150 °C for poorly crystallized kaolinites, it is possible to say that these samples exhibit well-crystallized kaolinite properties.

In TG studies; weight losses occur due to adsorbed and crystal water losses of kaolinite, and more weight loss occurs in poorly crystalline kaolinites. Adsorbed water and crystal water percentages are different for well-crystalline kaolinite and poorly crystalline kaolinite, while well-crystalline kaolinite loses 0.26 % weight loss when it loses its adsorbed water, the weight loss for poorly crystalline kaolinite is 0.74 %. On the other hand, while the weight loss for well-crystalline kaolinite due to the removal of crystal water from the structure is 13.11 %, this loss is 13.14 % for poorly crystalline kaolinite. The weight loss due to the endothermic peak in the 500–600 °C range is around 5 % (Ece et al., 2008).

4.4. Ceramic applications

In additions to mineralogical, geochemical analyses, reological and

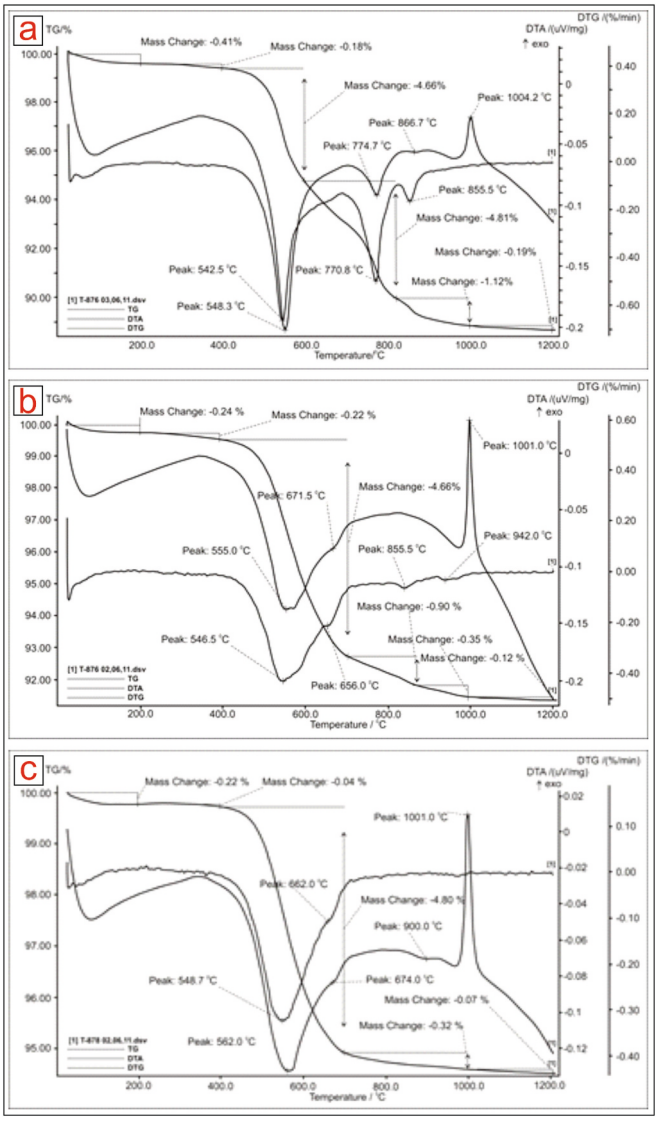

Fig. 5. a) DTA-TG curves of Kaolen 1, b) DTA-TG curves of Kaolin 3, c) DTA-TG curves of Kaolen 5.

firing properties (e.g., moisture, liter weight, viscosity, sieve balance, shrinkage, water absorption, glow loss, color (L, a, b), firing shrinkage, firing strength) were also performed on 6 characteristic samples (kaolin 1, 2, 3, 4, 5, 6) collected from the Sinandede kaolin formation in the study area and the results of kaolin samples are given in Table 2.

The <2 μm fraction was analysed from oriented aggregates under the following conditions: Air dried, solvated with ethylene glycol and heated. The mineralogical composition is composed of kaolinite with dickite, illite, smectite-chlorite, Ca-montmorillonite, alunite, halloysite, feldspar, quartz, opal CT, hematite, and anhydrite. The kaolin is the most clay mineral whereas quartz is the main impurity.

4.5. Geochemical analysis

In order to determine the geochemical properties of the kaolins and to reveal the elemental mobility during kaolinization, major, trace and rare earth element analyses were performed on 7 kaolin and 1 parent rock sample. The analytical results are presented in Table 3. SiO_2 values of the samples vary between 59.36 % and 76.97 %; Al_2O_3 values vary between 14.74 % and 28.36 %. Chemical Weathering Index (CIA) = $[(Al_2O_3)/(Al_2O_3 + CaO + Na_2O + K_2O)]x100]$ values indicate the degree of chemical weathering, and values greater than 80 % indicate

Table 2
The physical test results of kaolin samples.

Sample Nr.		SDK-1	SDK-2	SDK-3	SDK-4	SDK-5	SDK-6
Moisture		0.5	0.5	0.6	0.5	6	5.81
Liter Weıght (gr/lt)		1510	1512	1516	1520	1517	1512
Viscosıty (sn)		12	12	12	12	12	12
Sieve Remain (g)		1.6	2	1.8	1.6	2	1.9
Shrinkage (%)		0.91	1.63	0	0.27	0.36	0.09
Water Absorption (%)		25.15	23.88	21.93	23.62	20.49	20.48
Heating (%)		9.76	16.64	7.3	7.83	6.13	6.64
Color	L	91.9	91.8	91.29	91.44	92.83	92.25
	a	1.29	1.66	1.78	1.56	0.93	1.13
	b	3.74	4.9	4.82	4.49	4.95	2.06
Temperature/ Time (°C/ min.)		1203° – 35’	1203° – 35’	1203° – 35’	1203° – 35’	1203° – 35’	1203° – 35’
Baking Shrinkage		1.03	0.29	0.39	0.44	2.61	2.56
Baking Strength		23	22	18	13	38	92

feldspar alteration and chloritic or advanced argillic alteration (Nesbitt and Young, 1984). High CIA values ranging from 90.09 % to 99.66 % in the samples examined indicate high chemical weathering and argillic alteration.

4.6. Isotope analysis

Oxygen ($\delta^{18}O$), hydrogen (δD) and carbon ($\delta^{13}C$) isotope geochemistry of 5 kaolin samples from Sinandede kaolin deposit were analysed. The $\delta^{18}O$ values of the samples vary between +0.48 ‰ and − 4.96 ‰; δ values vary between −81.05 ‰ and − 89.97 ‰; and δ13C values vary between −25.70 ‰ and − 28.83 ‰ (VPDB) (Table 4). The $\delta^{18}O$-δD isotopic compositions of clays formed at high temperatures (hydrothermal) are on the left side of the S/H line and close to the meteoric water line (Sheppard et al., 1969; Taylor Jr., 1974; Decher, 1996; Sheppard and Gilg, 1996) because the δD and $\delta^{18}O$ values of clay minerals, where the isotopes stabilize at high temperatures, approach water. This distribution of isotope compositions refers to the change in the isotope composition of solutions due to different geological and geochemical events and indicates the activity of hydrothermal waters of meteoric origin (Taylor Jr., 1974; Ohmoto, 1986). Similarly, such a distribution of isotope compositions on the right side of the meteoric water line (positive δ18O shift) indicates the influence of temperature on mineral formation (Sheppard and Gilg, 1996).

5. Discussion

The mineral assemblage in the upper parts of the Sinandede kaolin deposit is kaolinite + quartz ± feldspar. In the north-northeast of the kaolin deposit; both in the upper and middle parts of the deposit (especially between 20 and 25 m); the typical mineral assemblage is kaolinite + quartz + alunite ± hematite. In the south-southwest; in the sections defined as silicified kaolin between 3 and 10 and 15–25 m between 3 and 10 and 15–25 m; a mineral assemblage in the form of quartz + kaolinite + opal-CT ± alunite ± anhydrite ± hematite is dominant, while in the lower sections a mineral assemblage in the form of kaolinite + quartz + illite ± Ca-montmorillonite ± feldspar is observed (Çoban et al., 2011).

The Sinandede kaolin deposit was formed as a result of hydrothermal alteration of Lower Miocene dacitic-rhyodacitic glassy-crystalline tuffs. The kaolin, with irregular pockets, lenses and (thin) veins, averages 15–20 m in thickness, according to 23 drill holes drilled to depths

Table 3
Major, trace and rare earth element contents of kaolin samples.

Sample Nr.	SDK-1	SDK-2	SDK-3	SDK-15	SDK-16	SDK-17	SDK-18	ANK
Major Oxides (% Weight)								
SiO_2	68.98	63.05	59.36	68.71	68.95	73.92	76.97	61.79
Al_2O_3	20.78	25.59	28.36	21.7	14.74	17.71	15.34	14.56
Fe_2O_3	0.26	0.15	0.14	0.34	0.27	0.12	0.39	4.89
MgO	0.005	0.005	0.01	0.005	0.03	0.005	0.005	3.46
CaO	0.06	0.05	0.16	0.04	0.08	0.05	0.06	4.36
Na_2O	0.01	0.005	0.02	0.02	0.52	0.05	0.01	2.29
K_2O	0.04	0.03	0.03	0.03	1.02	0.04	0.06	3.38
TiO_2	0.5	0.71	0.33	0.62	0.52	0.47	0.4	0.58
P_2O_5	0.15	0.16	0.3	0.14	0.16	0.16	0.13	0.20
MnO	0.005	0.005	0.005	0.005	0.005	0.005	0.005	0.09
Cr_2O_3	0.003	0.006	0.004	0.007	0.002	0.004	0.003	0.009
LOI	9.1	10.1	11.1	8.2	13.6	7.3	6.4	4.10
TOT/S	0.06	0.08	0.12	0.07	0.15	0.12	0.03	0.02
Total	99.91	99.91	99.92	99.90	100.02	99.97	99.82	99.76
Trace Elements (ppm)								
Ba	485	299	629	216	460	222	1367	1056
Co	0.1	0.1	0.1	0.4	0.3	0.1	0.7	10.5
Cs	0.1	0.05	0.1	0.05	2.8	0.1	0.6	3
Sc	7	9	5	8	9	11	4	15
W	2.1	3.3	3.3	6.6	1.9	3.9	1.5	1.9
Ga	21.5	30.9	26.2	35.2	16.2	21	11.7	16.2
Hf	5.2	6.7	3.5	6.5	5.2	5.5	4.4	4.5
Nb	13.5	17.9	11.1	16.4	13.6	11.7	10.5	12.6
Rb	0.8	0.7	0.8	0.7	25	0.7	3.7	122.3
Sr	667.7	836.9	820.8	857.2	338.3	676.6	572	444.1
Ta	1.1	1.6	1.3	1.5	1.3	1.2	1	0.9
Th	21.4	29.8	21	25	19.2	16.8	14.2	21.2
U	5.8	8.1	7.9	7.7	2.1	5.5	3.2	5.4
V	80	119	98	124	41	122	36	112
Zr	181.4	247.3	133.6	241.7	190.1	200	172.7	159.2
Y	5.3	7	9	7.8	8.1	8.2	6.2	22.2
Cu	2.9	2.1	1	9.7	1.5	1.3	1.7	6.5
Pb	7.9	8.7	4.4	15.1	6	3.9	9.8	21.3
Zn	1	1	0.5	2	0.5	0.5	1	52
Ni	0.4	0.4	0.3	0.3	0.5	0.3	0.9	3.7
As	25.1	4	4.6	5.8	1.8	2.1	6.2	2.4
Sb	0.1	0.05	0.1	0.2	0.05	0.05	0.05	0.1
Rare Earth Elements (ppm)								
La	34.9	45.1	69.3	37.5	46.9	42.3	24.6	39.9
Ce	72.9	83.9	135.2	77.4	117.9	91.3	50.6	78.3
Pr	9.44	8.23	11.23	7.03	14.46	10.91	6.72	8.34
Nd	40	28.5	30.7	22.8	60.3	44.7	36.1	30.05
Sm	5.26	3.72	4.11	3.21	11.99	7.3	8.17	5.47
Eu	0.69	0.47	0.68	0.45	1.82	1.09	1.43	1.1
Gd	2.42	1.79	3.07	1.97	6.66	3.57	4.27	4.72
Tb	0.27	0.24	0.42	0.29	0.67	0.4	0.48	0.72
Dy	1.31	1.29	1.93	1.57	2.54	1.72	1.96	3.93
Ho	0.2	0.27	0.37	0.29	0.33	0.27	0.28	0.76
Er	0.54	0.8	1.04	0.82	0.8	0.78	0.75	2.25
Tm	0.11	0.14	0.2	0.14	0.13	0.14	0.12	0.34
Yb	0.75	1.08	1.34	1.05	0.98	1.06	0.86	2.19
Lu	0.12	0.18	0.21	0.19	0.16	0.17	0.13	0.34
ΣREE	174.21	182.71	268.8	162.51	273.74	213.91	143.12	201.06
$(La/Lu)_{CN}$	31.16	26.87	35.39	21.15	31.41	26.67	20.27	12.56
$(La/Yb)_{CN}$	33.36	29.94	37.08	25.61	34.31	28.61	20.51	13.06
Y/Ho	26.5	25.92	24.32	26.89	24.54	30.37	22.14	29.21
Eu/Eu*	0.51	0.49	0.56	0.50	0.57	0.57	0.66	0.57
Ce/Ce*	0.96	1.21	1.07	1.08	1.10	1.01	0.94	0.61
Gd/Gd*	0i94	0.71	1.42	1.18	1.13	1.00	1.06	1.57
LREE/HREE	13.88	12.78	13.72	10.15	11.34	11.29	7.66	4.22
SiO_2/Al_2O_3	3.31	2.46	2.09	3.16	4.67	4.17	5.01	4.24
K_2O/Al_2O3	0.0019	0.0011	0.0010	0.0013	0.069	0.0022	0.0039	0.2321
CIA	99.47	99.66	99.26	99.58	90.09	99.21	99.15	59.21
A/B	3.25	2.40	2.08	3.09	4.65	4.08	4.92	5.29

LOI: Loss on Ignition, ANK: Bedrock; slightly altered samples (SDK16–17-18); highly altered samples (SDK1, SDK2, SDK3, SDK15), CIA: Chemical weathering index values, A/B = $(SiO_2 + Fe_2O_3 + MgO + Na_20 + CaO + K_2O) / (Al_2O_3 + TiO_2)$.

Table 4
Isotopic compositions of the studied kaolinites.

Sample Nr.	δD‰ (SMOW)	δ^{18}0‰ (SMOW)	δ^{13}C‰ (VPDB)
SDK-15	−84.06	+0.48	−28.83
SDK-16	−85.33	−0.98	−25.89
SDK-17	−81.05	−3.02	−27.47
SDK-18	−89.07	−3.97	−26.10
SDK-19	−87.76	−4.96	−25.70

ranging from 26.5 to 55 m. The kaolin bed, which contains opal bands ranging in thickness from 10 cm to 2 m, especially between 1 and 5, 15–19 and 32–35 m, is covered by a silicified cover ranging in thickness from 3 to 6 m. The kaolin deposit, which contains intense manganese-iron oxide in its fractures, is cut by thin clay and quartz veins developed in different directions (Çoban et al., 2011). According to XRD analysis, kaolinite, dickite, illite, smectite-chlorite and Ca-montmorillonite are the main clay minerals. Alunite, halloysite, feldspar, quartz, opal-CT, hematite, and anhydrite were included in the composition as non-clay minerals.

Chemical Weathering Index (CIA) values ranging from 90.09 % to 99.66 % in the kaolin samples studied indicate that the degree of chemical weathering is high (Nesbitt and Young, 1984). On the other hand, SiO_2/Al_2O_3 values ranging between 2.09 % and 5.01 % in the samples are higher than the theoretical kaolinite SiO_2/Al_2O_3 value (1.81), indicating that kaolinization is moderate and very fine quartz formation (Sousa et al., 2006; Erkoyun and Kadir, 2011; Ece et al., 2013; Çoban, 2015). The quartz and opal CT detected in most of the samples by XRD investigations support the high SiO_2/Al_2O_3 ratios. K_2O/Al_2O_3 values between 0.069 and 0.001 in the samples indicate that the kaolinization of the feldspars is complete (Bukalo et al., 2017). On the other hand, the increase in $(SiO_2 + Fe_2O_3 + MgO + Na_2O + CaO + K_2O) / (Al_2O_3 + TiO_2)$ ratios from less altered samples to highly altered samples is indicative of hydrothermal zonation in the kaolin deposit (Abedini and Calagari, 2015).

According to petrographic studies, sericitization of biotites in the tuffs, transformation of hornblende to sericite-chlorite, carbonation and silicification indicate that the tuffs were altered to varying degrees. The typical kaolinite+quartz±alunite paragenesis, the coexistence of kaolinite with opal CT, and the loose packing of regular-irregular book-shaped hexagonal kaolinite sheets in SEM studies indicate that the Sinandede kaolin deposit was formed in association with hydrothermal processes (Keller, 1976, 1978; Yılmaz et al., 2013).

DTA-TG curves of the kaolin samples examined are given in Fig. 5. For well-crystallized kaolinite, endothermic peaks reflecting the deterioration of the structure (loss of OH) are given as between 500 and 660 °C (Kakali et al., 2001; Kadir et al., 2022) and 630 °C (Mackenzie, 1970). Depending on the decrease in the peak temperature of the main water loss (dehydroxylation) in kaolinite as the structural regularity is deteriorated, this endothermic peak for poorly crystalline kaolinite was determined as 625 °C (Mackenzie, 1970). Similarly; It was determined that the strong endothermic peaks in the range of 530-700 °C indicate that the crystal structure water is removed from the structure (dehydration and decomposition of the structure) and weight loss occurs accordingly; the weight loss is greater in poorly crystalline kaolinites showing less pronounced endothermic peaks (Miyashiro, 1974). On the other hand; endothermic peaks reflecting dehydration and decomposition of the structure for dickite and nakrite occur at higher temperatures than for kaolinite (600–650 °C for dickite, 700 °C for nakrite) (Smykatz-Kloss, 1974).

In the DTA curves of the kaolin samples examined, the main endothermic peaks reflecting dehydration (OH output) and decomposition of the structure were found at 548 °C (Kaolen 1, narrow sharp peak), 555 °C (Kaolen 3, slightly flat peak), 562 °C (Kaolen 5, partially narrow sharp peak) (Fig. 5a,b,c). In kaolinitic clays, endothermic peaks lower than 580 °C are given as typical peaks for disordered kaolinite (Smykatz-Kloss, 1974). In all 3 samples examined, endothermic peaks are lower than 580 °*C. medium* strong exothermic peaks reflecting the formation of new crystal phases occur between 900 and 1000 °C (42); 940-1000 °C and 980-1005 °C (Smykatz-Kloss, 1974). The 900-1000 °C range is also valid for well-crystallized kaolinite (Kakali et al., 2001; Arslan et al., 2006). On the other hand, it is stated that the exothermic peaks at 1008-1010 °C indicate phase change for kaolinite. The exothermic peak value for well-crystallized dickite and nacrite is given as 940 ± 1 °C (Smykatz-Kloss, 1974). In the kaolin samples examined, the exothermic peaks indicating the collapse of the kaolinite crystal lattice structure and new phase crystallization are observed at 1001 and 1004 °C.

In TG studies; weight losses occur due to adsorbed and crystal water losses of kaolinite, and more weight loss occurs in poorly crystalline kaolinites. Adsorbed water and crystal water percentages are different for well-crystalline kaolinite and poorly crystalline kaolinite, while well-crystalline kaolinite loses 0.26 % weight loss when it loses its adsorbed water, the weight loss for poorly crystalline kaolinite is 0.74 %. On the other hand, while the weight loss for well-crystalline kaolinite due to the removal of crystal water from the structure is 13.11 %, this loss is 13.14 % for poorly crystalline kaolinite. The weight loss due to the endothermic peak in the 500–600 °C range is around 5 % (Ece et al., 2008). In the kaolin samples examined, the amounts of water lost due to the removal of adsorbed water were determined as 0.41 % for kaolen 1 sample, 0.24 % for kaolen 3 sample and 0.22 % for kaolen 5 sample and the total weight losses were determined as 9.18 %, 8.64 % and 5.45 %, respectively (Fig. 5a,b,c). When both DTA and TG curves were evaluated collectively, it was determined that the kaolinites were partly irregular, well crystallized and their grain sizes were variable.

In additions to mineralogical, geochemical analyses, reological and firing properties (e.g., moisture, liter weight, viscosity, sieve balance, shrinkage, water absorption, glow loss, color (L, a, b), firing shrinkage, firing strength) were also performed on 6 characteristic samples (kaolin 1, 2, 3, 4, 5, 6) collected from the Sinandede kaolin formation in the study area and the results of kaolin samples are given in Table 2.

The <2 μm fraction was analysed from oriented aggregates under the following conditions: Air dried, solvated with ethylene glycol and heated. The mineralogical composition is composed of kaolinite with dickite, illite, smectite-chlorite, Ca-montmorillonite, alunite, halloysite, feldspar, quartz, opal CT, hematite, and anhydrite. The kaolin is the most clay mineral whereas quartz is the main impurity.

The clay samples contain 5 % or more of Fe_2O_3 are red-firing clays, for those contain Fe_2O_3 between 1 and 5 % are B tan-burning clays and those contain less than 1 % of Fe_2O_3 are white firing clays (Murray, 2006). That's why, the high iron content of these clays (Table 3), they can be used for the production of fine ceramics, as well as, they could be considered as raw materials for structural ceramic products (Murray, 2006). Their chemical compositions are compared with some commercially known kaolin deposits of Europe and Türkiye in the ternary diagram silica-alumina- other oxides (Fig. 6). The figure displays that Sinandede clay samples are situated on mainly Latium kaolin deposits of Germany, which provides relatively uniform raw materials for ceramic industries. Properties such as water absorption, linear shrinkage and color measurements of the samples were analysed to define the firing properties of the Sinandede kaolin samples (Table 2). The results revealed that they can be utilized for additions of 10–15 % to wallfloor tile bodies. Water absorption and flexural strength are considered to be the most important properties of building ceramic products for civil construction, while linear shrinkage is a parameter that indicates the sintering mechanism and should be controlled to guarantee stability and avoid cracks in the product.

The K_2O/Al_2O_3 ratio gives information about the kaolinization process of feldspars, and if this ratio is greater than 0.1, the kaolinization of feldspars is incomplete (Bukalo et al., 2017). In the samples studied, this ratio varies between 0.001 and 0.069, indicating that kaolinization is complete. The theoretical SiO_2/Al_2O_3 value for kaolinite is given as 1.81 (Ekosse, 2001) and values higher than 1.81 indicate excess silica in

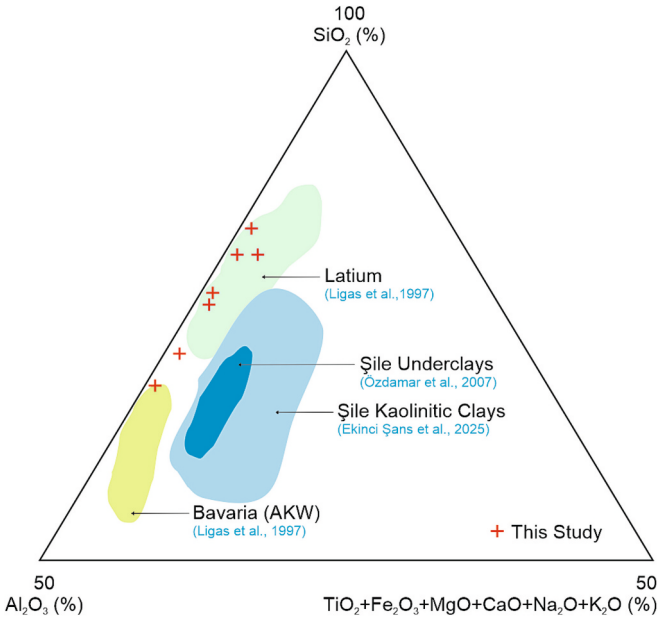

Fig. 6. SiO_2 (%) - Al_2O_3 (%) - $TiO_2 + Fe_2O_3 + MgO + CaO + Na_2O + K_2O$ (%) ternary diagram (Ligas et al., 1997; Özdamar et al., 2007; Ekinci Şans et al., 2025).

kaolinite (Sousa et al., 2006; Erkoyun and Kadir, 2011; Ece et al., 2013). The SiO_2/Al_2O_3 value in the samples varies between 2.09 and 5.01. This ratio varies between 4.17 and 5.01 in less altered samples (SDK16–17-18) and between 2.09 and 3.31 in highly altered samples (SDK 1,2,3,15). The $(SiO_2 + Fe_2O_3 + MgO + Na_2O + CaO + K_2O) / (Al_2O_3 + TiO_2)$ ratios vary between 4.08 and 4.92 in the less altered samples and between 2.08 and 3.25 in the highly altered samples and show an increase from the highly altered to the less altered section. These changes from less altered to more altered samples indicate the presence of hydrothermal zonation in the Sinandede kaolin deposit (Abedini and Calagari, 2015). High SiO_2/Al_2O_3 values and quartz and opal-CT minerals determined in the mineralogical composition support the high silica content. On the other hand, the negative correlation between Al_2O_3 and SiO_2, K_2O, TiO_2 and Fe_2O_3 (Fig. 7) indicates that these oxides (SiO_2, K_2O, TiO_2 and Fe_2O_3) are present in different phases rather than in the kaolin structure (Baioumy et al., 2021). The data obtained from drilling in the Sinandede kaolin deposit show that the amount of SO_3 varies between 0.08 % and 12.28 %, and the amount of SO_3 is higher in the northern and north-eastern parts of the deposit (Çoban et al., 2011). The high SO_3 values should be related to the presence of anhydrite and alunite as determined by XRD and SEM. Elemental mobility occurs during kaolinization, which develops due to progressive alteration, and the high consumption of Fe, Mg, Ca, Na, K, and Ti elements by transport from the kaolinization environment indicates that kaolinization is extensive (Murray and Keller, 1993; Nyakaıru et al., 2001). In the normalized major element exchange diagram of Sinandede kaolin samples with respect to bedrock (sample number: ANK), Al_2O_3 and Loss on Ignition (LOI) were enriched, but Fe_2O_3, MgO, CaO, Na_2O, K_2O and MnO losses occurred (Fig. 8a). TiO_2 and P_2O_5 were consumed very little and showed very little enrichment in some samples.

Alumina, which is enriched about 2 times in kaolin compared to the parent rock, is enriched in situ from the residual material that is not

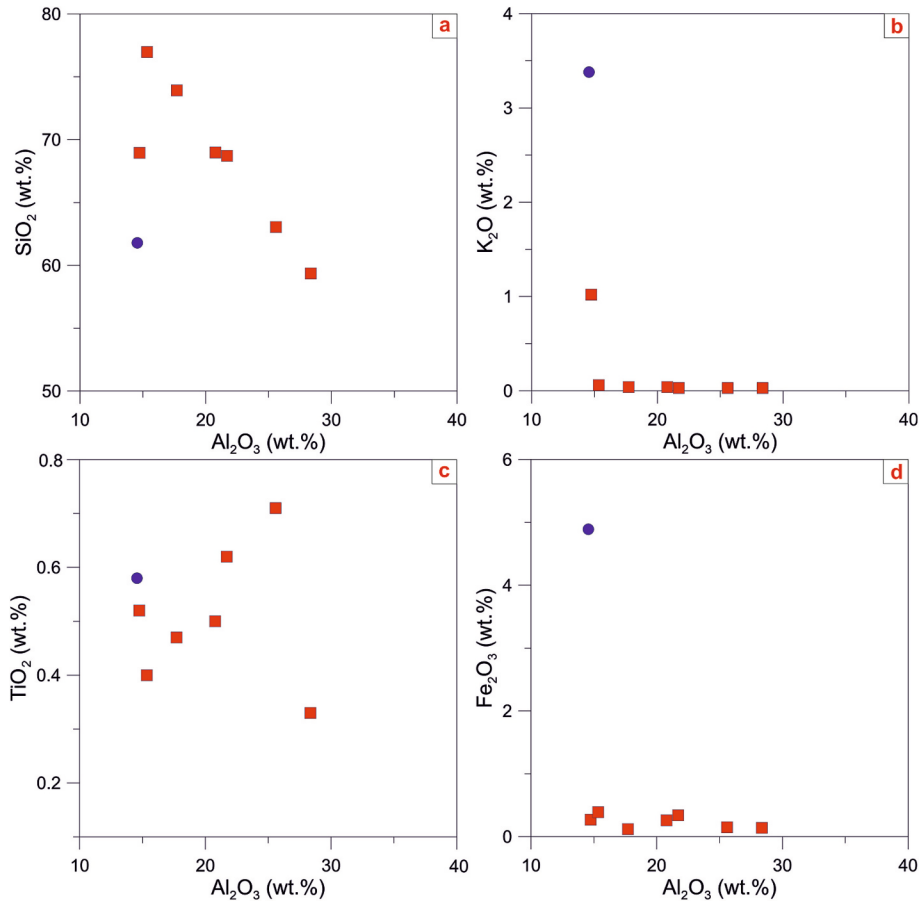

Fig. 7. Relationship between Al_2O_3 and SiO_2, K_2O, TiO_2 and Fe_2O_3 (●: parent rock). a) Al_2O_3-SiO_2 (r:-0.56), b) Al_2O_3-K_2O (r:-0.36), c) Al_2O_3-TiO_2 (r: −0.006), d) Al_2O_3-Fe_2O_3 (r: −0.43).

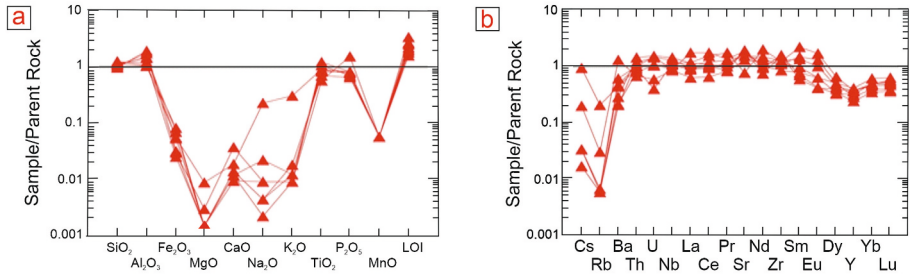

Fig. 8. a) The diagram of main element change during kaolinization, b) Change diagram of some trace elements during kaolinization.

dissolved due to alteration (White, 1983). P_2O_5 accumulated in some kaolin samples should be associated with phosphate-bearing alunites and/or authigenic phosphate minerals (Dill et al., 1995, 1997; Baioumy et al., 2021). On the other hand, high LOI values and enriched Al_2O_3 values together indicate new hydrous Al-silicates formed during alteration.

The behavior of trace elements during kaolinization gives information about the type of alteration and the degree of kaolinization. Accordingly, low trace element amounts in kaolin indicate high kaolinization, while different distributions of trace elements indicate differences in alteration. While the elements Zr, Ti, Nb, Cr, Y, W, and Yb are generally inactive during alteration (Maclean and Kranidiotis, 1987; Gifkins et al., 1995; Muchangos, 2006; Sousa et al., 2006); elements such as S, Ba, Sr, Cr, Nb, Ti, and REE enriched in kaolin as a result of alteration (Dill et al., 1995, 1997, 2000).

According to the trace element diagram of the kaolin samples normalized with respect to the parent rock; elements such as Cs, Rb, Ba, Y were depleted, whereas elements such as Th, U, Nb, Sr, and Zr were depleted in some samples and enriched in others. Of these, Sr and Zr seem to be completely accumulated in kaolin except for one sample (Fig. 8b). High Rb contents in kaolin are associated with K-feldspar, high Ba contents with K-feldspar, mica and alunite, and high Sr contents with plagioclase (Nyakaıru et al., 2001). Accordingly, kaolinization is high in samples with low Ba and Rb contents. The high Ba contents in SDK-3 and SDK-18 samples (compared to others) can be explained by the presence of alunite and partly by K-feldspar (Sousa et al., 2006). Sr, which shows about 2-fold enrichment, must have been retained in the kaolinite structure by adsorption. Components such as P_2O_5-S-Sr are found especially in kaolin deposits of hypogene origin and their content increases depending on the severity of alteration. The positive correlation between $(La/Yb)_N$ and the LOI indicates that alteration is increasing and accordingly LREE differentiation is higher than HREE and these relationships are characteristic for kaolin deposits of hypogene origin (Grecco et al., 2012).

In the binary diagrams between LOI and P_2O_5-S-Sr in the samples, it is seen that P_2O_5 and S contents are in an increasing trend from less

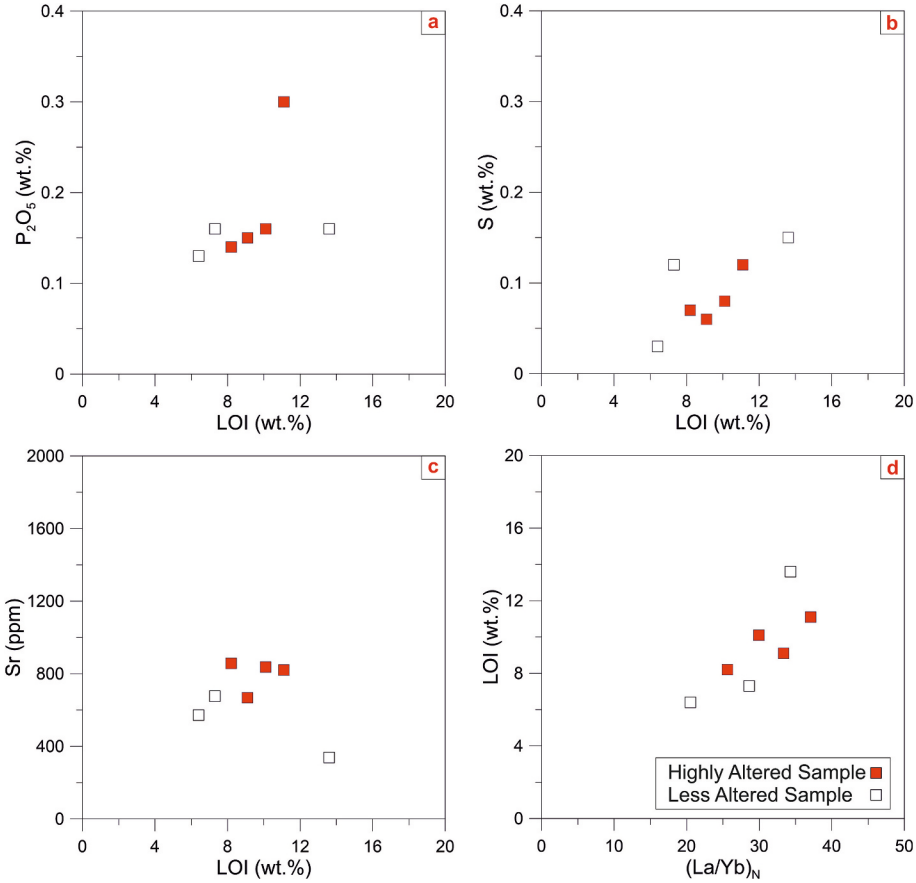

Fig. 9. Relationship between LOI and P_2O_5-S-Sr and $(La/Yb)_N$.

altered to more altered samples (Fig. 9a, b). There is no significant relationship is observed between the LOI value and Sr value (Fig. 9c). On the other hand; there is a high positive correlation (r = +0.79) between $(La/Yb)_N$ and LOI (Fig. 9d). These relationships indicate the effect of hypogene formation in Sinandede kaolin deposit.

The (Ba+Sr) - (Ce + Y + La), (Cr + Nb) - (Fe + Ti) and (Zr) - (TiO_2) diagrams can be used to distinguish supergene/hypogene kaolinization. Accordingly, Ba, Sr and S are enriched during hydrothermal alteration, while Cr, Nb, Ti and lanthanides are enriched mainly through weathering (Dill et al., 1997, 2000). In Sinandede kaolin samples, (Ba+Sr) values vary between 798 ppm and 1939 ppm; (Ce + Y + La) values vary between 81.4 ppm and 213.5 ppm; (Cr + Nb) values vary between 10.5 ppm and 17.9 ppm. The (Fe + Ti) values are low and vary between 0.47 and 0.96 wt%.

The (Cr + Nb) versus Ti + Fe diagram shows that the kaolins investigated are clustered in the hypogene kaolin area. The (Ba+Sr) contents in the samples are high and the (Ba+Sr)-(Ce + Y + La) exchange diagram shows that the samples (except SDK 16 and SDK 17 samples) are also located in the hypogene kaolin zone. On the other hand, the Zr-TiO_2 diagram shows that some of the samples (SDK2,15,17) are close to the mixed type area and the others are located in the hypogene area (Figs. 10a, b, c). Accordingly, hypogene and (partially) supergene effects played a role together in the formation of Sinandede kaolin deposit.

The behavior of REE in alteration processes depends on the properties of the altered host rock (mineralogy, chemical composition), the physico-chemical conditions of the alteration environment, the REE content of the hydrothermal solution and the transport of REE in the hydrothermal solution (Nesbitt, 1979; Humphris, 1984; Hill et al., 2000). REE released from primary minerals due to alteration can be adsorbed by Fe—Mn oxides and hydroxides, phosphate and clay minerals (Coppin et al., 2002; Kanazawa and Kamitani, 2006; Karadağ et al., 2009), resulting in REE enrichment in the altered product (Lopez et al., 2005; Kanazawa and Kamitani, 2006).

In order to determine the mobility of rare earth elements during kaolinization in the study area; the degree of fractionation = $(La/Yb)_{CN}$ and the diagram of REE normalized by chondrite were used and the correlation between ΣREE in kaolin and Al_2O_3, TiO_2 and P_2O_5 was examined. The "degree of REE fractionation", which indicates the concentration of LREE relative to HREE, is expressed as $(La/Yb)_{CN}$, and the larger the $(La/Yb)_{CN}$ ratio, the more mobilization of HREE (Goldstein and Jacobseny, 1988; Kundal et al., 2022). The evaluation of the $(La/Yb)_{CN}$ ratio together with the Eu anomaly provides information about the alteration environment conditions (Bau, 1991; Badurina and Segvic, 2022). Total REE content in kaolin samples varies between 143.12 ppm and 273.74 ppm. In the less altered samples (SDK 16–17-18), this amount varies between 143.12 and 273.74 ppm (mean 210.25 ppm), while in the highly altered samples (SDK 1–2–3-15) it varies between 162.51 and 268.8 ppm (mean 197.05 ppm). $(La/Yb)_{CN}$ values in the samples vary between 20.51 and 37.08 (mean 29.91). This ratio is between 20.51 and 34.31 (mean 27.81) in the less altered samples (SDK 16–17-18) and between 25.61 and 37.08 (mean 31.49) in the highly altered samples (Table 3). Accordingly, the larger $(La/Yb)_{CN}$ value in the highly altered samples indicates that HREE in the highly altered samples is more fractionated.

On the other hand; $(La/Lu)_{CN}$ ratios in kaolin samples vary between 20.27 and 35.39. This variability is related to the absorption of Lu more than La under acidic conditions (Fulignati et al., 1999). $(La/Lu)_{CN}$ ratios greater than 1 indicate that kaolinization occurs under the influence of low pH-low carbonate concentration or hydroxyl-containing fluids (Bau,

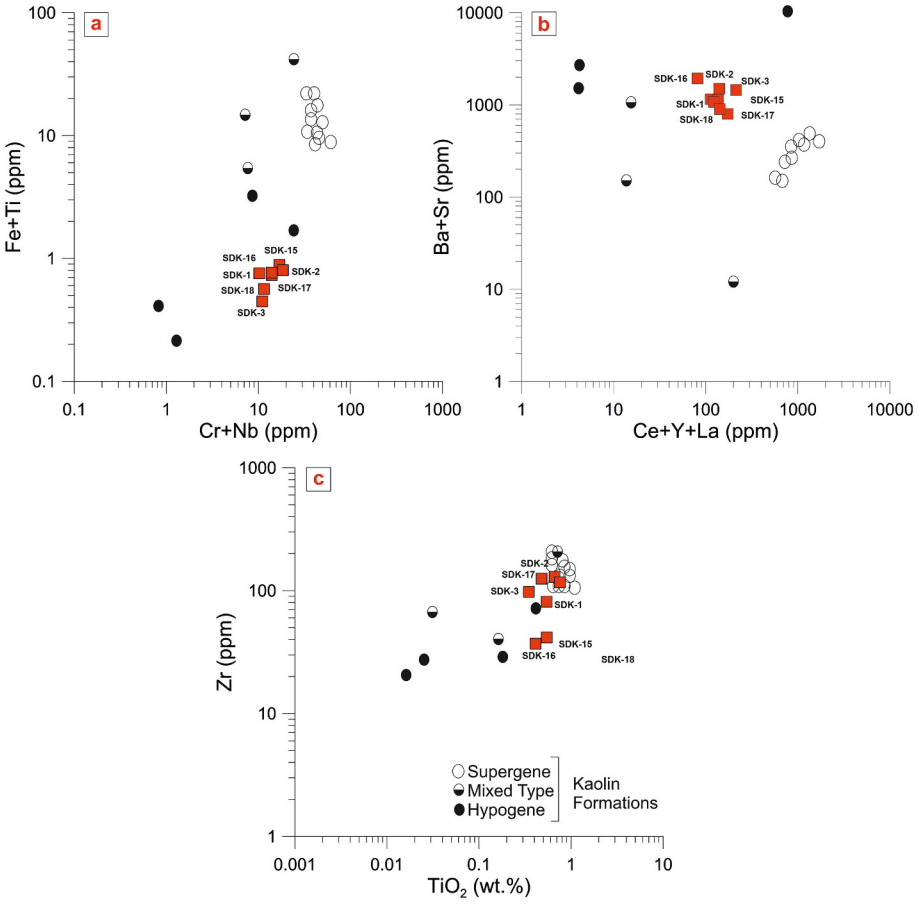

Fig. 10. The origin diagrams of kaolins (Dill et al., 1995, 2000).

1991; Kadir and Erkoyun, 2013; Abedini and Calagari, 2015). The chondrite normalized REE distributions of kaolins show that both LREE and HREE are enriched; LREE are more enriched than HREE and Eu shows negative anomaly and Gd shows (relative) positive anomaly (Fig. 11).

Minerals such as clay minerals, secondary phosphate minerals, Fe—Mn oxides and hydroxides, zircon, sphene, allanite, and garnet in alteration products cause enrichment of rare earth elements in alteration products (Nesbitt, 1979; Aja, 1998; Lopez et al., 2005; Kanazawa and Kamitani, 2006; Li and Zhou, 2020; Li and Zhou, 2023). Thus, the correlation calculations between ΣREE and major oxides are used to determine the REE mineralogy in kaolin deposits. If there is no correlation between ΣREE-Al_2O_3, it means that REE are not associated with the clay minerals present in the kaolin deposit and REE are retained by accessory minerals (Nouri and Masoumi, 2020; Baioumy et al., 2021). According to the correlation diagrams between ΣREE- P_2O_5; ΣREE-Al_2O_3; ΣREE-TiO_2 and ΣLREE-P_2O_5 of the Sinandede kaolin deposit shown in Fig. 12, there is a very low correlation between ΣREE and Al_2O_3 ($R^2 = 0.02$) (Fig. 12a). On the other hand; there is a low correlation between ΣREE and TiO_2 ($R^2 = 0.11$; Fig. 12b), a medium correlation between ΣLREE and P_2O_5 ($R^2 = 0.45$; Fig. 12c) and a medium correlation between ΣREE and P_2O_5 ($R^2 = 0.46$; Fig. 12d). Thus, it can be stated that the REE enriched in the kaolin under investigation are associated with phosphate-containing phases. P_2O_5 (0.46 %) determined in SEM examinations supports this situation. Y and Ho exhibit similar geochemical behavior and Y/Ho ratios provide information about the origin of the solution (Baioumy et al., 2021; Rieger et al., 2022). Accordingly, the Y/Ho value of crust-related fluids is close to the chondritic Y/Ho value (27.74) (Sun and McDonough, 1989; Zhang et al., 1994; Nozaki et al., 1997; Bau and Dulski, 1999). The Y/Ho values of the kaolin samples under investigation vary between 22.14 and 30.37 (Table 3) and the average is 25.81. Accordingly; it is possible to mention the contribution of hydrothermal solutions in the formation of Sinandede kaolin (Bau and Dulski, 1999; Baioumy et al., 2021; Rieger et al., 2022).

The evaluation of Eu and Ce anomalies together with chondrite normalized REE patterns reflects the nature of the kaolinization process and the nature of the solution and can be used to determine the origin of kaolin deposits. Accordingly, the enrichment of LREE over HREE, the presence of negative Eu anomalies and almost no Ce anomalies indicate the hydrothermal origin of the kaolin deposit (Baioumy et al., 2021). For the kaolin samples under investigation, the Eu anomaly (numerically) was calculated according to the formulas $(Eu/Eu^*) = (Eu_N)/[(Sm_N \times Gd_N)^{1/2}]$ and the Ce anomaly (numerically) was calculated according to the formulas $(Ce/Ce^*) = [(Ce_N)/[(La_N \times Pr_N)^{1/2}]$ (Liao et al., 2016) (N represents chondrite normalized values and C1 chondrite values are taken from Sun and McDonough (1989)). (Eu/Eu*) values <1 (Bea, 2004) or less than 0.85 (Kundal et al., 2022) indicate a negative anomaly. Negative Eu anomalies are associated with the alteration of plagioclase, potassium feldspar and hornblende (Arslan et al., 2006), high activity of complexing agents, high pH of the hydrothermal solution and increased oxygen fugacity (fO_2) in the hydrothermal system

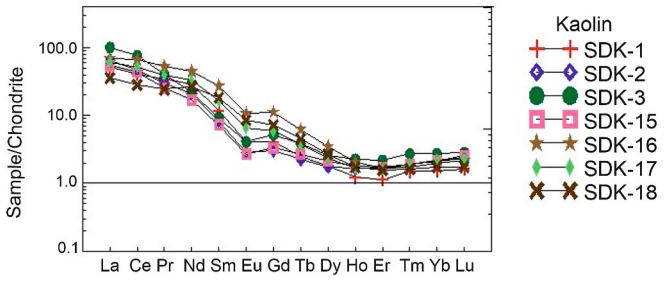

Fig. 11. Chondrite normalized diagram of REE (Chondrite values taken from (Sun and McDonough, 1989)).

(Sverjensky, 1984; Elderfield and Sholkovitz, 1987; Karakaya et al., 2012; Özdamar et al., 2014; Naseri et al., 2020). Similarly, negative Eu anomaly is observed in felsic rocks with high LREE/HREE ratio and is associated with the alteration of feldspar (plagioclase) (Liao et al., 2016).

Eu/Eu* values in the samples vary between 0.49 and 0.66 (average 0.55). This ratio, which is 0.57 in bedrock, varies between 0.57 and 0.66 in less altered samples and between 0.49 and 0.56 in highly altered samples (average 0.52), indicating the presence of fractionation and negative Eu anomaly with values less than 0.85 (Kundal et al., 2022).

Under normal natural oxidation-reduction conditions, Ce enrichment or depletion occurs (Semhi et al., 2009). Ce enrichment occurs as a result of the conversion of Ce^{3+} to Ce^{4+} under oxidizing conditions (McLennan, 1989). On the other hand, Ce^{3+} is more easily oxidized to Ce^{4+} under high oxygen fugacity (fO_2) conditions; Ce^{4+} is more easily adsorbed (and less migrated) by iron-manganese oxide/hydroxide than Ce^{3+} ($Ce/Ce^* > 1$) (Wang and Liang, 2015). Positive Ce anomalies are typical of residual or meteorically formed kaolin deposits (Cravero et al., 2001). A significant negative Ce anomaly ($Ce/Ce^* < 1$) represents (a) <0.5 (oxic conditions); (b) ~0.6–0.9 (suboxic conditions), and (c) ~0.9–1.0 (anoxic) seawater (Nyakaıru et al., 2001). Ce/Ce* values in kaolin samples range from 0.94 to 1.21 (average 1.05). This ratio, which is 0.61 in the bedrock, ranges from 0.94 to 1.10 (mean 1.016) in the less altered samples and from 0.96 to 1.21 (mean 1.08) in the highly altered samples. The Ce/Ce* values in the altered samples are higher than the Ce/Ce* values in the bedrock. Accordingly, although Ce/Ce* values between 0.94 and 1.21 indicate the presence of oxidizing conditions (meteoric water contribution and near-surface alteration) during Sinandede kaolin formation (Wang and Liang, 2015; Nouri and Masoumi, 2020), it is not possible to speak of a clear positive anomaly for the samples.

Furthermore, changes in Ce anomalies can be controlled by the breakdown of zircon by oxidizing acid liquids (Fulignati et al., 1999; Karakaya, 2006; Kadir et al., 2011; Abedini and Calagari, 2015). Accordingly, Zr contents gradually decrease from bedrock to altered product due to decreasing Ce/Ce* values from bedrock to altered product. Since this relationship between Ce/Ce* values and zircon contents is not observed in the Sinandede kaolin samples, the (very small) positive Ce anomaly in the samples must be related to iron oxide/hydroxides. Gd is classified as MREE or HREE and Gd anomaly can be found in groundwater and surface water (Nozaki et al., 2000; Möller et al., 2000; Rabiet et al., 2009). On the other hand, Gd complexes can dissolve in the presence of Cu, Y, and REE and exist as Gd^{3+} (Möller et al., 2011). The high Gd content of hydrothermal fluids and the high Ca content of bedrock (especially plagioclases) cause positive Gd anomalies in kaolin (Nouri and Masoumi, 2020).

The formula $Gd/Gd^* = Gd_N/0.33Sm_N + 0.67Tb_N$ was used to determine the Gd anomaly in the kaolin samples studied (Bau and Dulski, 1996; Kulaksız and Bau, 2007; Bobos and Gomes, 2021). (N represents chondrite normalized values and C1 chondrite values are taken from Sun and McDonough (1989)). The Gd/Gd* values in the samples vary between 1.57 in the bedrock, between 0.71 and 1.18 in the less altered samples (average 1.06) and between 1.00 and 1.13 in the highly altered samples (average 1.06). Accordingly, the Gd/Gd* value in kaolin samples (except SDK1 and SDK2 samples) is greater than 1 (average 1.06), indicating a positive Gd anomaly (Kulaksız and Bau, 2007).

According to geochemical studies, the mobilization of major, trace and rare earth elements as a function of progressive alteration during the kaolinization process by hydrothermal alteration of feldspars and volcanic glass, found as microliths and phenocrysts in volcanic rocks of neutral-acid composition, provides information about the degree and origin of kaolinization. Accordingly, kaolin becomes poorer in SiO_2, K_2O, Na_2O, CaO, Fe_2O_3, Cr, Nb, and Ti and richer in Al_2O_3, LOI, S, Ba, Sr, and LREE due to progressive alteration (Terakado and Fujitani, 1998; Dill et al., 1997, 2000; Grecco et al., 2012; Kadir and Erkoyun, 2013;

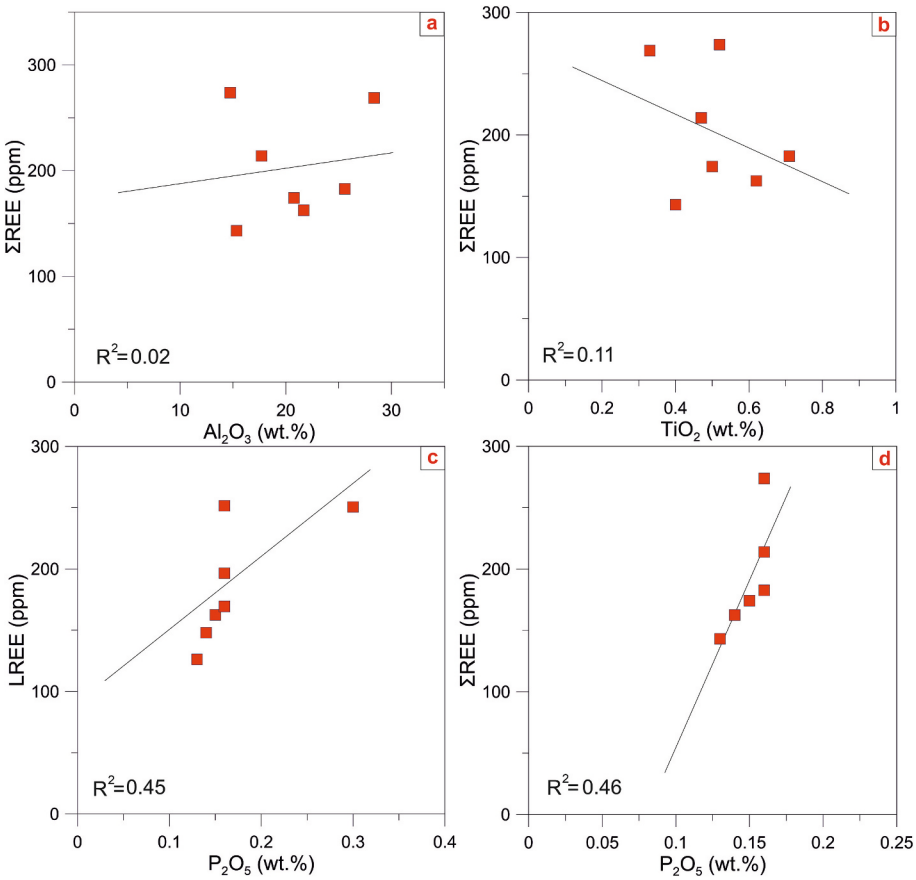

Fig. 12. Diagrams of a) ΣREE-Al_2O_3, b) ΣREE-TiO_2, c) LREE-P_2O_5, d) ΣREE-P_2O_5.

Abedini and Calagari, 2015; Nouri and Masoumi, 2020; Baioumy et al., 2021). Similarly, hydrothermal alteration of rhyolitic tuffs results in depletion of SiO_2, K_2O, CaO and Ba, but an increase in Al_2O_3 and LOI. The increase in Al_2O_3 and LOI indicates an increase in kaolinization (Papoulis and Tsolis-Katagas, 2001a, 2001b). On the other hand, the depletion of K, Na, Ca, Fe, and Mg indicates the formation of kaolinite under acidic conditions in an open hydrological system where hydrothermal solution is active (Yuan et al., 2014). According to the variation diagram normalized to the host rock, Sinandede kaolinite is enriched in Al_2O_3 and LOI, while impoverished in Fe_2O_3, MgO, CaO, Na_2O and K_2O. TiO_2 and P_2O_5 were consumed very little, and Al_2O_3, which was enriched about twice in kaolin, should have been enriched in situ due to alteration. On the other hand, the negative correlations between Al_2O_3 and SiO_2, K_2O, TiO_2 and Fe_2O_3 indicate that SiO_2, K_2O, TiO_2, and Fe_2O_3 are present in different phases rather than in the kaolin structure (Baioumy et al., 2021).

The trace element distributions in the examined kaolin samples do not show large variations and their enrichment in kaolin is generally low, indicating high kaolinization (Muchangos, 2006; Sayın, 2007). According to the trace element diagram normalized to bedrock, Cs, Rb, Ba, and Y are depleted and transported out of the system with kaolinization; Th, U, Nb, Sr, and Zr are enriched in some samples and depleted in others, highlighting hydrothermal alteration (Terakado and Fujitani, 1998; Yuan et al., 2014). High positive correlations between LOI and P_2O_5, S, Sr, and $(La/Yb)_{CN}$ in the samples indicate the hypogene origin of the Sinandede kaolin deposit (Grecco et al., 2012). SO_3 values ranging from 0.08 % to 12.28 % (Çoban et al., 2011) indicate the presence of S in the kaolin. S, thought to be of external origin, must have been used in the formation of alunite and anhydrite, as determined by XRD and SEM. The fact that kaolin samples are located in the hypogene and mixed-type formation regions in the (Ba+Sr)-(Ce + Y + La), (Cr + Nb)-(Fe + Ti), and (Zr)-(TiO_2) binary exchange diagrams, where hypogene/supergene kaolinization is distinguished, indicates that hypogene and supergene effects acted together in the formation of the Sinandede kaolin deposit (Dill et al., 1995, 2000).

The genetic characteristics of the Sinandede kaolin deposit are influenced by both hypogene and supergene processes. The presence of dickite alongside kaolin and the extensive hydrothermal alteration of feldspars and volcanic glass support the hypothesis of hypogene kaolinization. This interpretation is further substantiated by stable isotope compositions: $\delta^{18}O$ values ranging from −25.7 to −28.8 ‰ and δD values between −26.8 to −28.5 ‰ suggest equilibration with hydrothermal fluids at elevated temperatures, indicative of a hypogene origin. Additionally, the relatively consistent rare earth element (REE) distribution patterns and the occurrence of negative cerium (Ce) anomalies in certain samples imply fluid–rock interactions under reducing, hydrothermal conditions.

Supergene alteration is evident in the upper sections of the deposit, where halloysite is found in association with kaolin, Fe—Mn oxide coatings have formed, and partial leaching of alkalis occurs. The enrichment of silica phases, such as opal-CT and quartz, in surface samples, along with varying lanthanum/lutetium (La/Lu) ratios, indicates weathering-related overprinting and near-surface mobilization. Thus, while kaolinization is primarily hypogene in origin, the infiltration of meteoric water and low-temperature alteration have resulted in a supergene overprint that has modified the primary mineral assemblage and geochemical signatures in the shallow layers of the deposit.

Rare earth element geochemistry, REE patterns, and Eu and Ce anomalies are used to interpret solution and kaolinization origins rather than bedrock composition (Bau and Dulski, 1999; Nyakaıru et al., 2001; Baioumy et al., 2021; Rieger et al., 2022). Accordingly, if the LREE enrichment in kaolin is higher than the HREE enrichment and there is a

negative Eu anomaly (Dill et al., 1995; Grecco et al., 2012; Kadir and Erkoyun, 2013; Kadir et al., 2014) and there is no positive Ce anomaly, it is said that the kaolinization is of hydrothermal origin (Baioumy et al., 2021). Total REE content in Sinandede kaolin samples varies between 143.12 ppm and 273.74 ppm. The chondrite-normalized plot shows that the enrichment in LREE is higher than in HREE, with a negative Eu anomaly and a (relatively) positive Gd anomaly. The $(La/Yb)_{CN}$ ratio (degree of fractionation) values (between 20.51 and 37.08), which express the concentration of LREE relative to HREE, indicate that HREE is more fractionated in the samples (Kundal et al., 2022). On the other hand, $(La/Lu)_{CN}$ ratios greater than 1 and ranging between 20.27 and 35.39 in the samples indicate that kaolinization occurred under the influence of low pH, low carbonate content or hydroxyl-containing fluids (Bau, 1991; Kadir and Erkoyun, 2013; Abedini and Calagari, 2015). Numerous explanations have been proposed in the literature to account for the variations in La/Lu ratios, including the selective adsorption of LREEs as opposed to HREEs on clay minerals, the presence of secondary iron-manganese oxides, and partial leaching during weathering. In the case of the Sinandede kaolin deposit, the elevated La/Lu ratios are primarily ascribed to the preferential adsorption of LREE on the surfaces of kaolin and dickite, as demonstrated by the prominent development of these phases in the XRD patterns and SEM observations. In contrast, there is scant evidence of significant iron-manganese oxide accumulation or extensive supergene leaching, suggesting that these processes exerted a minor influence. Consequently, the observed La/Lu fractionation is largely attributable to the impact of clay mineral surfaces under hydrothermal conditions, with only minor alterations from near-surface weathering processes. Eu/Eu* values less than 0.85 and between 0.49 and 0.66 indicate the presence of a negative Eu anomaly (Kundal et al., 2022). Considering the high LREE/HREE ratios (average 11.55) in the kaolin samples and the loss of Fe, K, Rb, and Ba despite the enrichment of Al during the kaolinization process, the negative Eu anomaly must have occurred due to the destruction of minerals such as K-feldspar, plagioclase and hornblende in the dacite-rhyodacite characterized tuffs that were altered due to the increasing degree of alteration by acidic hydrothermal fluids (Arslan et al., 2006; Abedini and Calagari, 2015; Liao et al., 2016). Furthermore, Ce/Ce* values ranging from 0.94 to 1.21 (average 1.05) and greater than 1 in kaolin samples indicate (partially) positive Ce anomaly and the presence of oxidizing conditions (meteoric water contribution or near-surface alteration) during kaolin formation (Wang and Liang, 2015; Nouri and Masoumi, 2020). Similarly, Gd/Gd* values greater than 1 (mean 1.06) indicate the presence of a Gd anomaly (Kulaksız and Bau, 2007). Considering the Gd value of 1.57 ppm in the bedrock, it can be stated that the positive Gd anomaly in kaolin samples is related to the (partial) enrichment of Gd in kaolin (Nouri and Masoumi, 2020) and/or the contribution of meteoric water (Rabiet et al., 2009) released as a result of weathering of Ca-bearing minerals (especially plagioclases) in the bedrock composition rather than Gd in hydrothermal solutions.

Analyzing the distribution of the samples in the δD versus $\delta^{18}O$ diagram, it can be seen that the samples are located in the hydrothermal zone to the left of the supergene (S)/hypogene (H) line and away from the meteoric water line, close to the left of the kaolinite line (Hayba et al., 1985), which is in equilibrium with waters at temperatures above 100 °C (Fig. 13). The fact that the isotopic composition distribution of the investigated samples lies to the right of the meteoric water line (in the hydrothermal zone) and shows a positive $\delta^{18}O$ shift compared to the meteoric water line indicates that the temperature during the kaolinite formation process was high. On the other hand, low isotopic ranges indicate that the isotopic composition of the kaolinites has not changed (Faure and Mensing, 2004). The crystallization temperatures of the studied kaolinites were calculated using the formula $T(K) = \sqrt{\frac{3.04x10^6}{\delta^{18}O_k - 0.125x\delta D_k + 7.04}}$ (Gilg and Sheppard, 1996; Raphalalani et al., 2019; Baioumy et al., 2021). Accordingly, the crystallization temperatures of

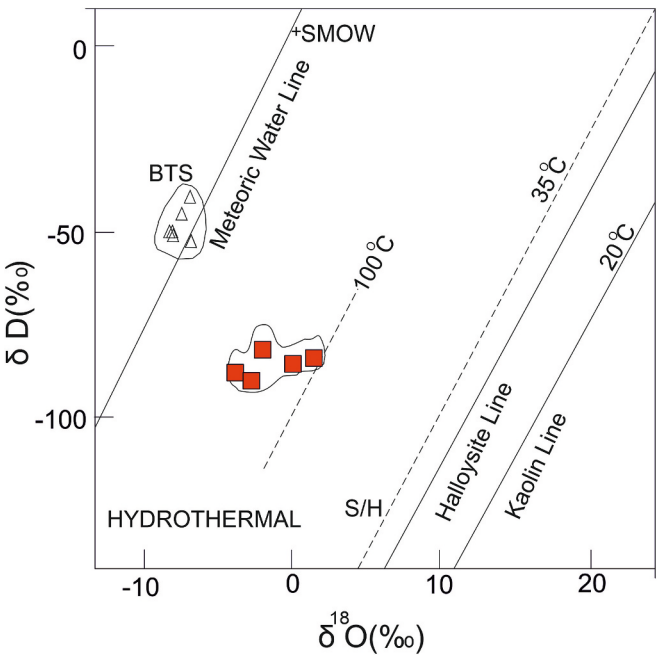

Fig. 13. δD-$\delta^{18}O$ isotopic composition diagram of the kaolinites under investigation. (Meteoric Water Line (Craig, 1961); Kaolinite line in equilibrium with waters at temperatures above 100 °C (Hayba et al., 1985); Supergene/Hypogene line (Sheppard and Gilg, 1996); Kaolinite 20 °C line (Savin and Epstein, 1970); BTS: Isotopic composition of thermal waters of Balıkesir (Bigadiç-Sındırgı) (Mutlu, 2007)).

kaolinites vary between 82 °C and 173 °C, with an average of 111 °C.

One of the stable carbon isotopes, ^{13}C (the heavy carbon isotope) is most abundant in oxidized forms of carbon (CO_2 and carbonates) and in biogenic organic origin ($\delta^{13}C$: −25 ‰) (Hoefs, 2009). They are commonly used as geochemical traces of biological processes at local and global scales (Planavsky et al., 2014) and to distinguish biogenic from abiogenic origin (Criss, 1999; Hoefs, 2009; Busigny, 2014). The Mediterranean Climate Zone, where atmospheric CO_2 levels are high and warm and humid climatic conditions prevail (Guo et al., 2012). The $\delta^{13}C$ values of modern terrestrial C3 plants (trees, heaths and shrubs adapted to cool and humid conditions) in the region range from −20 ‰ to −37 ‰ (VPDB), with an average of-28.5 ‰ (VPDB) (Deines, 1980; O'Leary, 1988; Farquhar et al., 1989; Cerling et al., 1993; Hoefs, 2009; Kohn, 2010). The carbon isotope compositions of hydrothermal fluids mixed with meteoric waters fed by C3 plants are in the range of $\delta^{13}C$: −27 ‰ to −29 ‰ (Pasquier-Cardin et al., 1999; Fiebig et al., 2019). The $\delta^{13}C$ values in the kaolin samples examined vary between-25.70 ‰ and-28.83 ‰ (VPDB) (Table 4); the average value is-27.26 ‰. These values are consistent with the 13C values of both C3 plants and hydrothermal waters mixed with meteoric water fed with C3 plants.

Stable isotope (δD, $\delta^{18}O$, $\delta^{13}C$) studies in clay minerals are used to determine the environment and conditions of clay mineral formation and to determine the source of the fluid that forms clay minerals (Savin and Epstein, 1970; Sheppard and Gilg, 1996; Hoefs, 2009; Bozkaya et al., 2019). The $\delta^{18}O$-δD ratios of clays formed at high temperatures (hydrothermal) are in the region between the kaolinite line and the meteoric water line and close to the meteoric water line; the $\delta^{18}O$-δD ratios of clays formed at lower temperatures (surface weathering-weathering) are close to the kaolinite lines (Sheppard et al., 1969; Taylor Jr., 1974, 1979; Decher, 1996; Sheppard and Gilg, 1996).

The $\delta^{18}O$-δD isotopic compositions of Sinandede kaolin samples are located in the hydrothermal zone to the left of the "100°C kaolinite line" in the section between the kaolinite line (Hayba et al., 1985), which is in equilibrium with waters at temperatures above 100 °C, and the meteoric water line. The crystallization temperatures of the kaolinites vary

between 82 °C and 173 °C (average 111 °C). The wide range of temperature values should indicate changes in the isotopic composition of the solutions due to different geological and geochemical events (Taylor Jr., 1974). Low isotopic ranges, on the other hand, indicate that the isotopic compositions of the kaolinites do not change (Faure and Mensing, 2004). On the other hand, $\delta^{13}C$ (VPDB) values between-25.70 % and-28.83 % (VPDB) in kaolen samples are compatible with $\delta^{13}C$ (VPDB) values of hydrothermal waters mixed with meteoric water fed by C3 plants (Pasquier-Cardin et al., 1999; Fiebig et al., 2019), indicating a contribution of meteoric water in the Sinandede kaolin formation. The small positive Ce and Gd anomalies and the distribution of the samples in the Dill et al. (1995) diagram, indicating the presence of hypogene supergene mixing, support the meteoric water contribution. Sinandede kaolin was formed as a result of post-magmatic hydrothermal activity at temperatures above 100 °C and under the influence of supergene conditions.

6. Conclusions

The following conclusions were reached according to the mineralogical, thermal, physical and geochemical properties of the samples taken from the Sinandede kaolin deposit:

1. The Sinandede kaolin deposit was formed by hydrothermal alteration of Lower Miocene dacitic-rhyodacitic tuffs
2. The mineralogical studies revealed presence kaolinite with dickite, illite, smectite-chlorite, Ca-montmorillonite, alunite, halloysite, feldspar, quartz, opal CT, hematite and anhydrite in the Sinandede kaolin deposite.
3. Technological properties showed that Sinandede kaolin-containing formulations have acceptable technological properties compared to standard porcelain tile bodies.
4. They could be used as raw material in floor tile manufacturing by ceramic industries.
5. It formed as a result of post-magmatic hydrothermal activities at temperatures above 100 °C.
6. Both hypogene and supergene effects played a role together in the formation of Sinandede kaolin deposit.

CRediT authorship contribution statement

Fazlı Çoban: Writing – original draft, Data curation. **Şenel Özdamar:** Writing – review & editing, Writing – original draft, Validation, Data curation, Conceptualization. **Oral Sarıkaya:** Software, Data curation. **Gökhan Büyükkahraman:** Writing – original draft, Investigation, Data curation. **Zeynep Döner:** Writing – review & editing. **Naşide Merve Sütçü:** Writing – review & editing.

Declaration of competing interest

The authors declare that they have no known competing financial interests or personal relationships that could have appeared to influence the work reported in this paper.

References

Abedini, A., Calagari, A.A., 2015. Geochemical characteristics of the Abgarm kaolin deposit, NW Iran. N. Jb. Geol. Paläont. (Abh.) 278 (3), 335–350.

Aja, S.U., 1998. The sorption of rare earth element, Nd to kaolinite at 25°C. Clays ClayMinerals. 46, 103–109.

Akdeniz, N., Konak, N., 1979. Menderes Masifi'nin Simav dolayındaki kaya birimleri ve metabazik, metaultrabazik kayaların konumu. Türk. Jeol. Kurumu Bül. 22, 175–184.

Arslan, M., Kadir, S., Abdioglu, E., Kolaylı, H., 2006. Origin and formation of kaolin minerals in saprolite of Tertiary alkaline volcanic rocks, Eastern Pontides, NE Turkey. Clay Miner. 41 (2), 597–617.

Badurina, L., Segvic, B., 2022. Assessing trace-element mobility during alteration of rhyolite tephra from the Dinaride Lake System using glass-phase and clay-separate laser ablation inductively coupled plasma mass spectrometry. Clay Miner. 57, 1–6.

Baioumy, H., Farahat, M., Arifin, M.H., Anuar, M.N.A.B., Al-Kahtany, K., 2021. Hypogene kaolin deposits from felsic intrusive rocks (Peninsular Malaysia) with special reference to rare earth elements and stable isotopes geochemistry. Geosci. J. 25 (6), 863–876.

Bau, M., 1991. Rare-earth element mobility during hydrothermal and metamorphic fluid-rock interaction and the significance of the oxidation state of europium. Chem. Geol. 93 (3–4), 219–230.

Bau, M., Dulski, P., 1996. Anthropogenic origin of positive gadolinium anomalies in river waters. Earth Planet. Sci. Lett. 143, 245–255.

Bau, M., Dulski, P., 1999. Comparing yttrium and rare earths in hydrothermal fluids from the Mid-Atlantic Ridge: implications for Y and REE behavior during near vent mixing and for the Y/Ho ratio of Proterozoic seawater. Chem. Geol. 155, 77–90.

Bea, F., 2004. Geochemistry of the Lanthanide Elements C1-condrites Silicate Earth. Seminario SEM 12, Depósito legal: CA-602/ISSN: 1698–5478, 8 p.

Bobos, I., Gomes, C., 2021. Mineralogy and Geochemistry (HFSE and REE) of the Present-Day Acid-Sulfate Types Alteration from the Active Hydrothermal System of Furnas Volcano, São Miguel Island. The Azores Archipelago Iuliu. Minerals 11 (4), 335.

Bozkaya, Ö., Bozkaya, G., Yılmaz, H., Hozatlıoğlu, D., Banks, D.A., 2019. The origin, age and duration of hydrothermal alteration associated with iron skarn mineralization determined from clay/phyllosilicate minerals, Bizmişen-Erzincan. East-Central Turkey. Ore Geology Reviews 115, 103179.

Brown, G., Brindley, G.W., 1980. In: Brown, G. W.Brindley ve G. (Ed.), X-ray diffraction procedures for clay mineral identification. Crystal structure of clay minerals and their X–ray identification. Mineralogical Society, London, s.495.

Bukalo, N.N., Georges-Ivo, E., Ekosse, E., John Odiyo, O., Jason, S., 2017. Geochemistry of Selected Kaolins from Cameroon and Nigeria, Review Article. Open Geoscience 9, 600–612.

Busigny, V., 2014. Stable Isotopes. Encyclopedia of Astrobiology. https://doi.org/10.1007/978-3-642-27833-45083-1. Springer-Verlag Berlin Heidelberg.

Çelik Karakaya, M., Karakaya, N., Temel, A., Yavuz, F., 2021. Mineralogical and geochemical properties and genesis of kaolin and alunite deposits SE of Aksaray (Central Turkey). Appl. Geochem. 124, 104830.

Cerling, T.E., Wang, Y., Quade, J., 1993. Expansion of C4 ecosystems as an indicator of global ecological change in the late Miocene. Nature 361, 344–345.

Çoban, F., 2015. Danaçayır (Sındırgı-Balıkesir) kaolin yatağının mineralojik-jeokimyasal özellikleri: Kaolinleşme sırasındaki majör; eser ve nadir toprak elementlerinin mobilizasyonu. Çukurova Üniversitesi Mühendislik Mimarlık Fakültesi Dergisi 30 (2), 311–332.

Çoban, F., Ece, Ö.I., Yavuz, O., Özdamar, Ş., 2002. Petrogenesis of volcanic rocks, and clay mineralogy and genesis of underclays, Şile Region, İstanbul, Turkey. Neues Jahrbuch für Mineralogie – Abhandlungen 178, 1–25.

Çoban, F., Büyükkahraman, G., Cincioğlu, D., 2011. Sinandede (Sındırgı-Balıkesir) Bölgesi Kaolen Oluşumlarının Mineralojik-Jeokimyasal Özellikleri ve Endüstriyel Kullanım Parametrelerinin Belirlenmesi. Balıkesir Üniversitesi Bilimsel Araştırma Projesi, p. 115. Proje No: 2010/13.

Çoban, F., Büyükkahraman, G., Bircan, C., 2012. Sinandede (Sındırgı-Balıkesir) Bölgesi Kalk-Alkalen Volkanizmasının ve İlişkili Kaolen Oluşumlarının Jeokimyasal Özellikleri. V. Ulusal Jeokimya Sempozyumu (Poster Bildiri), Denizli.

Coppin, F., Berger, G., Bauer, A., Castet, S., Loubet, M., 2002. Sorption of lanthanides on smectite and kaolinite. Chem. Geol. 182, 57–68.

Craig, H., 1961. Isotopic variations in meteoric waters. Science 133 (3465), 1702–1703.

Cravero, F., Dominguez, E., Iglesias, C., 2001. Genesis and Applications of the CerroRubio Kaolin Deposit, Patagonia (Argentina). Appl. Clay Sci. 18, 157–172.

Criss, R.E., 1999. Principles of stable isotope distribution. Oxford Univ Press, New York.

Das, S.K., Dana, K., Singh, N., Sarkar, R., 2005. Shrinkage and strength behaviour of quartzitic and kaolinitic clays in wall tile compositions. Appl. Clay Sci. 29 (2), 137–143.

Decher, A., 1996. Bentonite der Inset Milos/Griechenland Mineralogie, Geochemie and Entstehung. Bowie ihre geotechnische Verwendung, p. 210. PhD thesis.

Deines, P., 1980. The isotopic composition of reduced organic carbon. In: Fritz, P., Fontes, J.C. (Eds.), Handbook of Environmental Isotope Geochemistry I, The Terrestrial Environment. Elsevier, Amsterdam, pp. 329–406.

Dewey, J.F., 1988. Extensional collapse of orogens. Tectonics 7 (6), 1123–1139.

Dill, H.G., 2016. Kaolin: Soil, rock and ore: From the mineral to the magmatic, sedimentary and metamorphic environments. Earth Sci. Rev. 161, 16–129.

Dill, H.G., Weiser, T., Bernhardt, I.R., Riera Kilibarda, C., 1995. The Composite Gold Antimony Vein Deposit at Kharma (Bolivia). Econ. Geol. 90 (51–66), 42.

Dill, H.G., Bosse, R., Henning, H., Fricke, A., 1997. Mineralogical and Chemical Variations in Hypogene and Supergene Kaolin Deposits in a Mobile Fold Belt the Central Andes of Northwern Peru. Mineral. Deposita 32, 149–163.

Dill, H.G., Bosse, H.R., Kassbohm, J., 2000. Mineralogical and Chemical Studies of Volcanic-Related Argillaceous Industrial Minerals of the Central American Cordillera (Western El Salvador). Econ. Geol. 95, 517–538.

Ece, Ö.I., Schroeder, P.A., Smilley, M.L., M., J., 2008. Acid-sulphate hydrothermal alteration of andesitic tuffs and genesis of halloysite and alunite deposits in the Biga Peninsula. Turkey, Clay Minerals 43, 281–315.

Ece, Ö.I., Ekinci, B., Schroeder, P.A., Douglas, C., Esenli, F., 2013. Origin of he Düvertepe kaolin-alünite deposits in Simav Graben, Turkey: Timing and styles of hydrothermal mineralization. Journal of Vocanology and Geothermal Research 255, 57–78.

Ekinci Şans, B., Sarıkaya, O., Esenli, F., Özdamar, Ş., Tunçdemir, H., Karadoğan, Ü., Kumral, M., 2025. Mineralogy and geochemistry of kaolinitic clays in the Şile Neogene Basin (İstanbul, Türkiye). Bulletin of the Mineral Research and Exploration 178, 14–32.

Ekosse, G.E., 2001. Provenance of he Kgwakgwe kaolin deposit in southeastern Botswana and its possible utilization. Appl. Clay Sci. 20, 137–152.

Elderfield, H., Sholkovitz, E.R., 1987. Rare earth elements in the pore waters of reducin nearshore sediments. Earth Planet. Sci. Lett. 82 (3–4), 280–288.
Ercan, T., Çevikbaş, A., Günay, E., Ateş, M., Can, B., Küçükayman, A., Erkan, M., 1984. Bigadiç çevresinin (Balıkesir) Jeolojisi ve Magmatik Kayaçların Petrolojisi. Türkiye Jeoloji Kurultayı Bülteni 5, 75–85.
Erkoyun, H., Kadir, S., 2011. Mineralogy, micromorphology, geochemistry and genesis of a hydrothermal kaolinite deposit and altered Miocene host volcanites in the Hallaçlar area, Uşak, western Turkey. Clay Miner. 46, 241–448.
Erkül, F., Helvacı, C., Sözbilir, H., 2005. Evidence for two episodes of volcanism in the Bigadiç borate basin and tectonic implications for western Turkey. Geol. J. 40, 545–570.
Farquhar, G.D., Ehleringer, J.R., Hubick, K.T., 1989. Carbon isotope discrimination and photosynthesis. Annu. Rev. Plant Physiol. Plant Mol. Biol. 40, 503–537.
Faure, G., Mensing, T.M., 2004. Isotopes: Principles and Applications. John Wiley and Sons, Hoboken, p. 897.
Fiebig, J., Stefansson, A., Ricci, A., Tassi, F., Viveiros, F., Silva, C., Lopez, M.T., Schreiber, C., Hofmann, S., Mountain, W.B., 2019. Abiogenesis not required to explain the origin of volcanic-hydrothermal hydrocarbons. Geochemical Perspective Letters. II, 23–27.
Fulignati, P., Gioncada, A., Sbrana, A., 1999. Rare-element (REE) behaviour in the alteration facies of the active magmatic-hydrothermal system of Vulcano (Aeolian Islands, Italy). J. Volcanol. Geotherm. Res. 88, 325–342.
Garbarino, C., Masi, U., Padalino, G., Palomba, M., 1994. Geochemical features of the kaolin deposits from Sardina (Italy) and genetic implications. Chem. Erde 54, 213–233.
Gifkins, C., Herrmann, W., Large, R., 1995. Altered Volcanic Rocks. A Guide Description and İnterpretation. University Tasmania, Australia, pp. 123–136.
Gilg, H.A., Sheppard, S.M.F., 1996. Hydrogen isotope fractionation between kaolinite and water revisited. Geochim. Cosmochim. Acta 60, 529–533.
Goldstein, S.J., Jacobseny, S.B., 1988. REE in the Great Whale River estuary, northwest Quebec. Earth Planet. Sci. Lett. 88, 241–252.
Grecco, L.E., Marfil, S.A., Maiza, P.J., 2012. Mineralogy and geochemistry of hydrothermal kaolins from the Adelita mine, Patagonya (Argentina); relation to other mineralization in the area. Clay Miner. 47, 131–146.
Guo, R.Z., Hu, F.C., Xiao, Z., Bin, Y.X., Qian, X., PinkYu, Z., 2012. Spatial and temporal variations of C3/C4 relative abundance in global terrestrial ecosystem since the Last Glacial and its possible driving mechanisms Chinese. Sci. Bull. 57 (31), 4024–4035.
Hayba, D.O., Bethke, P.M., Heald, P., Faley, N.K., 1985. Geologic, mineralogic and geochemical characteristics of volcanic-hosted epithermal precious-metal deposits. In: Berger, B.R. and Bethke, P.M. (eds.), Geology and Geochemistry of Epithermal Systems. Rev. Econ. Geol. 2, 129–167.
Hill, G., Worden, R.H., Meighan, I.G., 2000. Geochemical evolution of a palaeolaterite: the Interbasaltic Formation. Northern Ireland. Chemical Geology 166 (1–2), 65–84.
Hoefs, J., 2009. Stable Isotope Geochemistry, Eighth edition. Springer.
Humphris, S.E., 1984. The Mobility of the Rare Earth Elements in the Crust. In: Henderson, P. (Ed.), Rare Earth Element Geochemistry. Elsevier, Amsterdam, The Netherlands, pp. 317–342.
Kadir, S., Erkoyun, H., 2013. Genesis of the hydrothermal Karaçayır kaolinite deposit in Miocene volcanics and Palaeozoic metamorphic rocks of the Uşak Güre Basin, western Turkey. Turk. J. Earth Sci. 22 (3), 444–468.
Kadir, S., Erman, H., Erkoyun, H., 2011. Mineralogical and geochemical characteristics and genesis of hydrothermal kaolinite deposits within Neogene volcanites, Kutahya (western Anatolia). Turkey. Clays and Clay Minerals 59 (3), 250–276.
Kadir, S., Külah, T., Eren, M., Önalgil, N., Gürel, A., 2014. Mineralogical and geochemical characteristics and genesis of the Güzelyurt alunite-bearing kaolinite deposit within the Late Miocene Gördeles ignimbrite, central Anatolia. Turkey. Clays and Clay Minerals 62 (6), 477–499.
Kadir, S., Ateş, H., Erkoyun, H., Külah, T., Esenli, F., 2022. Genesis of alunite-bearing kaolin deposit in Mudamköy member of the Miocene Göbel Formation, Mustafakemalpaşa (Bursa). Turkey. Applied Clay Science 221, 106407.
Kakali, G., Perraki, T., Tsivilis, S., Badogiannis, E., 2001. Thermal treatment of kaolin: The effect of mineralogy on the puzzolanic activity. Appl. Clay Sci. 20, 73–80.
Kanazawa, Y., Kamitani, M., 2006. Rare earth minerals and resources in the world. J. Alloys Compd. 408, 1339–1343.
Karadağ, M., Küpeli, Ş., Arık, F., Ayhan, A., Zedef, V., Döyen, A., 2009. Rare earth element (REE) geochemistry and genetic implications of the Mortaş bauxite deposit (Seydişehir-Konya, Southern Turkey). Geochemistry 69 (2), 143–159.
Karakaya, M.Ç., 2006. Kil Minerallerinin Özellikleri ve Tanımlama Yöntemleri. Bizim Büro Basımevi, Ankara, pp. 491–537.
Karakaya, M.Ç., Karakaya, N., Küpeli, Ş., Yavuz, F., 2012. Mineralogy and geochemical behavior of trace elements of hydrothermal alteration types in the volcanogenic massive sulfide deposits. NE Turkey. Ore Geology Reviews. 48, 197–224.
Keller, W.D., 1976. Scan electron micrographs of kaolins collected from diverse environments of origin-1. Clay Clay Miner. 24, 107–113.
Keller, W.D., 1978. Classification of Kaolins Exemplified by Their Textures in Scan Electron Micrographs. Clay Clay Miner. 26 (1), 1–20.
Kohn, M.J., 2010. Carbon isotope compositions of terrestrial C3 plants as indicators of (paleo)ecology and (paleo)climate. Proceedings of the National Academy of Sciences of the USA 107, 19691–19695.
Kulaksız, S., Bau, M., 2007. Contrasting behaviour of anthropogenic gadolinium and natural rare earth elements in estuaries and the gadolinium input into the North Sea. Earth Planet. Sci. Lett. 260, 361–371.
Kundal, N.S., Chowdhary, N., Kumar, S., 2022. Geochemistry of bentonitized tuff band of outer NW Himalaya, Jammu and Kashmir, India. Indian Academy of Sciences. J. Earth Syst. Sci. 131 (2), 110.
Laçin, D., Aysal, N., Öngen, S., 2021. Geological mineralogical and technological properties of Oligocene–Miocene clay deposits in altered volcanic rocks for the ceramic industry (Western Anatolia, Turkey). Arab. J. Geosci. 14 (18), 1904.
Li, M.Y.H., Zhou, M.F., 2020. The role of clay minerals in formation of the regolith-hosted heavy rare earth element deposits. Am. Mineral. 105 (1), 92–108.
Li, M.Y.H., Zhou, M.F., 2023. Physicochemical variation of clay minerals and enrichment of rare earth elements in regolith-hosted deposits: exemplification from the Bankeng Deposit in South China. Clay Clay Miner. 71 (3), 362–376.
Liao, Z., Hu, W., Cao, J., Wang, X., Yao, S., Wu, H., Wan, Y., 2016. Heterogeneous volcanism across the Permian–Triassic Boundary in South China and implications for the Latest Permian Mass Extinction: New evidence from volcanic ash layers in the Lower Yangtze Region. J. Asian Earth Sci. 127, 197–210.
Ligas, P., Uras, I., Dondi, M., Marsigli, M., 1997. Kaolinitic materials from Romana (north-western Sardinia, Italy) and their ceramic properties. Appl. Clay Sci. 12, 145–163.
Lopez, J.M.G., Bauluz, B., Nieto, C.F., Oliete, A.Y., 2005. Factors controlling the trace elements distribution in fine grained rocks: The Albian Kaolinite rich deposits of the Oliete Basin (NE Spain). Chem. Geol. 214, 1–19.
Mackenzie, R.C., 1970. Differential Thermal Analysis. Academic Press, London.
Maclean, W.I., Kranidiotis, P., 1987. Immobile Elements as Monitors of Mass Transfer in Hydrothermal Alteration: Phelps Dodge Massive Sulfide Deposit, Matagami, Quebec. Econ. Geol. 82, 951–962.
McKenzie, D., 1972. Active tectonics of the Mediterranean region. Geophys. J. Int. 30 (2), 109–185.
McLennan, M.S., 1989. Rare earth elements in sedimentary rocks: Influence of provenance and sedimentary prcesses. In: Lipin, B.R., McKay, G.A. (Eds.), Geochemistry and Mineralogy of Rare Earth Elements. The Mineralogical Society of America, pp. 169–196.
Miyashiro, A., 1974. Volcanic rocks series in island arcs and active continental margins. Am. J. Sci. 274, 321–355.
Möller, P., Dulsky, P., Bau, M., Knappe, A., Pekdeger, A., Sommer-von Jarmerstedet, C., 2000. Anthropogenic gadolinium as a conservative tracer in hydrology. J. Geochem. Explor. 69-70, 409–414.
Möller, P., Knappe, A., Dulski, P., Pekdeger, A., 2011. Behavior of Gd DTPA in simulated bank filtration. Appl. Geochem. 26 (1), 140–149.
Muchangos, C.A., 2006. The Mobility of Rare-Earth Elements in the Process of Alteration of Rhyolitic Rocks to Bentonite (Lebombo Volcanic Mountainous Chain, Mozambique). Journal of Gechemical Exploration 88, 300–303.
Murray, H.H., 2006. Applied clay mineralogy: occurrences, processing and applications of kaolins, bentonites, palygorskitesepiolite, and common clays, vol. 2. Elsevier.
Murray, H.H., Keller, D.W., Murray, H.H., Wayne, B., Harvey, C., 1993. Kaolin Genesis and Utilitization, 1. The Clay Minerals Society Special Publ., pp. 1–24. Kaolins, Kaolins, and Kaolins.
Mutlu, H., 2007. Constraints on the origin of the Balıkesir thermal waters (Turkey) from stable isotope (δ18O, δD, δ13C, δ34S) and major-trace element compositions. Turk. J. Earth Sci. 16, 13–32.
Naseri, H., Jamadi, M., Radmard, K., Alavi, G., 2020. Mineralogy and geochemistry of rare earth elements in the Moyil Valley alteration zones, Meshkinshahr (northwest Iran). Geologos 26 (3), 219–231.
Nesbitt, H.W., 1979. Mobility and fractionation of rare earth elements during weathering of a granodiorite. Nature 279, 206.
Nesbitt, H.W., Young, G.M., 1984. Prediction of Some Weathering Trends of Plutonic and Volcanic Rocks Based on Thermodynamic and Kinetic Considerations. Geochim. Cosmochim. Acta 48, 1523–1534.
Nouri, T., Masoumi, R., 2020. Geochemical and industrial properties of the Kejal kaolin deposit, NW Iran. Turk. J. Earth Sci. 29, 325–346.
Nozaki, Y., Zhang, J., Amakawa, H., 1997. The fractionation between Y and Ho in the marine environment. Earth Planet. Sci. Lett. 148, 329–340.
Nozaki, Y., Lerche, D., Alibo, D.S., Tsutsumi, M., 2000. Dissolved indium and rare earth elements in three Japanese rivers and Tokyo Bay: Evidence for anthropogenic Gd and In. Geochim. Cosmochim. Acta 64, 3975–3982.
Nyakairu, A.W.G., Koeberl, C., Kurzweil, H., 2001. The Buwambo kaolin deposit in central Uganda: Mineralogical and chemical composition. Geochem. J. 35, 245–256.
Ohmoto, H., 1986. Stable isotope geochemistry of ore deposits. In: Taylor, J.W., O'Neil Jr., H.P. (Eds.), Stable Isotopes in High Temperature Geological Processes, vol. 16. Reviews in Mineralogy, Valley, pp. 491–559.
Okay, A.I., Tüysüz, O., 1999. Tethyan sutures of northern Turkey. In: Durand, B., Jolivet, L., Horvath, F., Seranne, M. (Eds.), The Mediterranean Basins: Tertiary Extension within the Alpine Orogeny, 156. Geological Society of London, Special Publication.
Okut, M.D., Demirhan, M., Köse, Z., 1978. Kütahya ili Emet-Simav ilçeleri kaolen zuhurları ve dolaylarının jeoloji raporu. MTA Raporu No: 6309.
O'Leary, M.H., 1988. Carbon isotopes in photosynthesis. BioScience 38, 328–336.
Özdamar, Ş., Ece, Ö.I., Kayacı, K., Küçüker, A.S., 2007. Mineralogical and Technological Properties of Underclays In Şile Region Istanbul Turkey. Industrial Ceramics 27 (3), 1–11.
Özdamar, Ş., Ece, Ö.I., Uz, B., Boylu, H.Ü., Yanık, G., 2014. Element mobility during the formation of the Uzunisa-Ordu bentonite, NE Turkey, and potential applications. Clay Miner. 49, 609–633.
Papoulis, D., Tsolis-Katagas, P., 2001a. Formation of alteration zones and kaolin genesis, Limnos Island, northeast Aegean Sea, Greece. Clay Miner. 43, 631–646.
Papoulis, D., Tsolis-Katagas, P., 2001b. Kaolinization process in the rhyolitic rocks of Kefalos, Kos Island, Aegean Sea, Greece. Bull. Geol. Soc. Greece 867–874. Proceedings of the International Congress, Athens, Greece. 24/3.
Pasquier-Cardin, A., Allard, P., ferreira, T., Hatte, C., Coutinho, R., Fontugne, M., Jaudon, M., 1999. Magma-derived CO2 emissions recorded in 14C and 13C content

of plants growing in Furnas caldera, Azores. J. Volcanol. Geotherm. Res. 92, 195–207.
Pickering, K.T., Marsh, N.G., Dickie, B., 1993. Data Report: in Organic Major, Trace And Rareearth Element Analyses of the Muds And Mudstones From Site 808. Proc. Ocean Drill. Program Sci. Results 131, 427–432.
Planavsky, N., Partin, C., Bekker, A., 2014. Carbon isotopes as a geochemical tracer. Springer-Verlag, Encylopedia of astrobiology.
Rabiet, M., Brissaud, F., Seidel, J.L., Pistre, S., Elbaz-Poulichet, F., 2009. Positive gadolinium anomalies in wastewater treatment plant effluents and aquatic environment in the Hérault watershed (South France). Chemosphere 75 (8), 1057–1064.
Raphalalani, A., Ekosse, Georges-Ivo, Odiyo, J., Ogola, J., Bukalo, N., 2019. Trace Element and Stable Isotope Geochemistry of Lwamondo and Zebediela Kaolins. Limpopo Province, South Africa: Implication for Paleoenvironmental Reconstruction, Minerals 9 (93), 1–19.
Rieger, P., Magnall, J.M., Gleeson, S.A., Oelze, M., Wilke, F.D.H., Lilly, R., 2022. Differentiating between hydrothermal and diagenetic carbonate using rare earth element and yttrium (REE+Y) geochemistry: a case study from the Paleoproterozoic George Fisher massive sulfide Zn deposit, Mount Isa, Australia. Mineral. Deposita 57, 187–206.
Savin, M.S., Epstein, S., 1970. The oxygen and hydrogen isotope geochemistry of clay minerals. Geochim. Cosmochim. Acta 34, 25–42.
Sayın, A.S., 2007. Origin of Kaolin Deposits: Evidence from the Hisarcık (Emet-Kütahya) deposits, Western Turkey. Turk. J. Earth Sci. 16, 77–96.
Semhi, K., Chaudhuri, S., Clauer, N., 2009. Fractionation of rare-earth elements in plants during experimental growth in varied clay substrates. Appl. Geochem. 24, 447–453.
Şengör, A.C., Yilmaz, Y., 1981. Tethyan evolution of Turkey: a plate tectonic approach. Tectonophysics 75 (3–4), 181–241.
Seyitoglu, G., Scott, B.C., Rundle, C.C., 1992. Timing of Cenozoic extensional tectonics in west Turkey. J. Geol. Soc. Lond. 149 (4), 533–538.
Sheppard, S.M.F., Gilg, H.A., 1996. Stable isotope geochemistry of clay minerals. Clay Miner. 31, 1–24.
Sheppard, S.M.F., Nielsen, R.L., Taylor, H.P., 1969. Oxygen and hydrogen isotope ratios of clay minerals from porphyry copper deposits. Econ. Geol. 64, 755–777.
Smykatz-Kloss, W., 1974. Differantial thermal analysis application and results in mineralogy. Springer-Verlag, p. 185.
Sousa, L.J.D., Varajo, C.D.F.A., Yvon, J., 2006. Gechemical Evolution of He Capim River Kaolin, Northern Brazil. J. Geochem. Explor. 88, 329–331.
Spears, D.A., Kanaris-Sotiriou, R., 1979. A geochemical and mineralogical investigation of some British and other European tonsteins. Sedimentology 26 (3), 407–425.
Sun, S.S., McDonough, W.F., 1989. Chemical and isotopic systematics of oceanic basalts: implication for mantle composition and processes. A.D. Saunder and M.J. Norry (Editors). Magmatism in the Ocean Basins, Geological Society Special Publication 42, 313–345.
Sverjensky, D.A., 1984. Europium redox equilibria in aqueous solution. Earth Planet. Sci. Lett. 67, Issue 170-78.
Taylor Jr., H.P., 1974. The application of oxygen and hydrogen isotope studies to problems of hydrothermal alteration and ore deposition. Econ. Geol. 69, 843–883.
Terakado, Y., Fujitani, T., 1998. Behavior of the rare earth elements and other trace elements during interactions between acidic hydrothermal solutions and silicic volcanic rocks, southwestern Japan. Geochim. Cosmochim. Acta 62 (11), 1903–1917.
Ünal, A., 1972. Hisaralan Kaplıcaları Civarının Jeotermal Alan Olanakları Hakkında Rapor. MTA Raporu 5974.
Ünal Ercan, H., Ece, Ö.I., Çiftçi, E., Aydın, A., 2022. Comparison of epithermal kaolin deposits from the Etili Area (Çanakkale, Turkey): mineralogical, geochemical, and isotopic characteristics. Clay Clay Miner. 70 (5), 753–779.
Wang, L., Liang, T., 2015. Geochemical fractions of rare earth elements in soil around a mine tailing in Baotou. China. Nature Scientific Reports. 5, 12483.
White, A.F., 1983. Surface Chemistry and Dissolution Kinetics of Glassy Rocks at 25oC. Geocimica Cosmochimica Acta. 47, 805–815.
Williams, L.A., Parks, G.A., Crerar, D.A., 1985. Silica diagenesis,I. Solubility Controls. J. Sediment. Petrol. 55, 301–311.
Wilson, M.J.A., 1987. Handbook of Determinative Methods in Clay Mineralogy. Blackie, London, p. 308.
Yanık, G., Esenli, F., Uz, V., Esenli, V., Uz, B., Külah, T., 2010. Ceramic properties of kaolinized tuffaceous rocks in Kesan region, Thrace. NW Turkey. Applied Clay Science 48 (3), 499–505.
Yanık, G., Ceylantekin, R., Taşçı, E., 2018. The Gümüşköy (Kütahya, Turkey) kaolin deposit and its ceramic properties. Clay Miner. 53 (3), 515–524.
Yılmaz, H., Sönmez, N.F., Akay, E., Şener, K.A., Tufan, T.S., 2013. Low-Sülfidation Epithermal Au-Ag Mineralization in the Sındırgı District, Balıkesir Province, Turkey. Turk. J. Earth Sci. 22, 485–522.
Yuan, Y., Guanghai, S., Mengchu, Y., Yinuo, W., Zhaochong, Z., Anjie, H., Jiajing, Z., 2014. Formation of a hydrothermal kaolinite deposit from rhyolitic tuff in Jiangxi. China. Journal of Earth Science 25 (3), 495–505.
Zhang, J., Amakawa, H., Nozaki, Y., 1994. The comparative behaviors of yttrium and lanthanides in the seawater of the North Pacific. Geophys. Res. Lett. 21, 2677–2680.